Title
Trabecular Microarchitecture, Endplate Failure, and the Biomechanics of Human Vertebral Fractures

Author
Fields, Aaron Joseph

Publication Date
2010

Peer reviewed|Thesis/dissertation

Trabecular Microarchitecture, Endplate Failure, and the Biomechanics of Human Vertebral Fractures

by

Aaron Joseph Fields

A dissertation submitted in partial satisfaction of the

requirements for the degree of

Doctor of Philosophy

in

Engineering – Mechanical Engineering

in the

Graduate Division

of the

University of California, Berkeley

Committee in Charge:

Professor Tony M. Keaveny, Chair
Professor Panayiotis Papadopoulos
Professor Mohammad Reza Kaazempur Mofrad

Fall 2010

Trabecular Microarchitecture, Endplate Failure, and the Biomechanics of Human Vertebral Fractures

by

Aaron Joseph Fields

ABSTRACT

Trabecular Microarchitecture, Endplate Failure, and the Biomechanics of Human Vertebral Fractures

by

Aaron Joseph Fields

Doctor of Philosophy in Engineering – Mechanical Engineering

University of California, Berkeley

Professor Tony M. Keaveny, Chair

Knowledge of the biomechanical behavior of the human vertebra is fundamental to improving clinical assessment of vertebral fracture risk and diagnosis of osteoporosis. In this context, the focus of this dissertation is to enhance the current understanding of the biomechanical mechanisms of vertebral strength and the etiology of vertebral fractures.

Combining the latest advances in micro-computed tomography, high-resolution finite element modeling, and biomechanical testing, we found that variation in vertebral strength across individuals was primarily due to the variation in the bone volume fraction of vertical trabeculae. This is because the major load paths were parallel columns of vertically-oriented bone. A new microarchitecture parameter, the vertical tissue fraction, was developed to reflect these findings. Whereas the role of traditional microarchitecture parameters in vertebral strength was mediated by bone mass and density, the role of this new parameter was independent of bone mass and density. From a biomechanics perspective, the vertical tissue fraction thus represents a mechanistic aspect of trabecular microarchitecture with the most potential for microarchitecture analysis of bone strength.

The work presented in this dissertation has also provided substantial insight into the etiology of vertebral fractures. We found that due to the variation in failure mechanisms between porous and dense vertebrae, the amount of tissue yielding that occurred during a mechanical overload of the vertebra was up to 5 times lower in porous vertebrae than in dense vertebrae. This illustrates a new aspect of vertebral fragility: as bone density decreases with aging and disease, not only is the vertebra becoming weaker, but it is also becoming much less structurally robust. Unique evidence was also obtained to help explain why the endplates are frequently involved in osteoporotic vertebral fractures. A detailed comparison of the biomechanical behavior of the endplates, cortical shell, and trabecular bone revealed that the endplates are at the highest risk of failure due to the development of high tensile strains, and that the development of such high tensile strains is directly associated with the material behavior of the intervertebral disc.

In closure, this dissertation answers fundamental questions regarding the role of trabecular microarchitecture in explaining the variation in vertebral strength across individuals, and provides new insight into the etiology of age-related vertebral fractures. This work also outlines areas of research to further advance our understanding of vertebral fracture etiology and describes a systematic approach for identifying architectural determinants of bone strength that could be used at other anatomic sites.

_____

Tony M. Keaveny

Dissertation Committee Chair

TABLE OF CONTENTS

LIST OF FIGURES

LIST OF TABLES

ACKNOWLEDGEMENTS

First and foremost, I would like to thank my advisor, Professor Tony Keaveny, for mentoring me during my graduate career at Berkeley. His guidance has been truly invaluable; moreover, I greatly admire Tony's dedication to his students and his infectious enthusiasm for research. I feel incredibly fortunate to have embarked on research in the field of Orthopaedic Biomechanics under his tutelage.

Second, I would like to thank the past and present members of the Orthopaedic Biomechanics Laboratory for creating a fun and collaborative atmosphere. Among all of the OBLers, I would especially like to thank Sarah Easley. She has been a wonderful friend and colleague, and I cannot thank her enough for the endless hours of discussion about research and coursework (and cooking and backpacking!). That I am really going to miss her companionship in the research lab is an understatement. I owe a great deal of thanks to Grant Bevill, Senthil Eswaran, and Carolyn Sparrey—they were always eager to aid me in troubleshooting problems and to provide advice for navigating the often-murky waters of graduate school. Thanks also to John Christiansen, Wes Jackson, Mike Jekir, Shashank Nawathe, Javier Reina, Arnav Sanyal, and Jesse Woo for their help and support. Three undergraduate students—Gideon Lee, Prem Nagarathnam, and Thanos Rossopoulos—assisted me with various aspects of the finite element modeling, and it was a pleasure getting to know them and working with them. I would like to acknowledge the expertise of Ed Guo and Sherry Liu, with whom I collaborated for the work involving trabeculae segmentation. Thanks also to Michael Liebschner for his help micro-CT imaging.

Third, I would like to acknowledge the funding sources for this research. Funding was provided by the National Institutes of Health (NIH AR049828, AR043784, and AR051376). Computational resources were provided by the National Partnership for Advanced Computational Infrastructure (UCB-266) and in part by the National Science Foundation through the TeraGrid program (TG-MCA00N019). Along these lines, I am very grateful for the folks working behind the scenes in San Diego and Austin—the ticketmasters. Their dedication is what really makes finite element analysis in the cloud possible.

On a more personal note, I would like to thank Sara Atwood for her kindness and friendship throughout my time here. Her students are incredibly lucky to have her as their professor.

Finally, I am eternally grateful to my family—to my parents for their love and encouragement, and to my sister for always watching out for her little brother. To Heidi—your love and friendship over the years has influenced my life in more ways than can be stated.

1. INTRODUCTION

The healthy human skeletal system is well adapted to performing a wide range of activities. A critical aspect governing skeletal adaptation is bone remodeling: continuous remodeling and turnover of the bone tissue at the cellular level ensures the bone structure is most suited to the external loads. However, imbalance in bone remodeling due to aging and disease can compromise skeletal integrity. Osteoporosis is a metabolic disease characterized by an imbalance in bone turnover that results in accelerated bone loss and deterioration of bone microarchitecture. This low bone mass and deteriorated microarchitecture causes a reduction in bone strength and an associated increase in fracture risk. According to the National Osteoporosis Foundation, over 2 million osteoporosis-related fractures occur annually in the United States. The most common locations for fracture are the vertebral body (700,000 annually), distal radius (400,000 annually), and proximal femur (300,000 annually) [1]. The estimated direct expenditures for these fractures is $19 billion, and both the incidence of osteoporotic fracture and the associated costs are expected to increase as the size of the elderly population continues to grow. All told, osteoporosis is currently considered a major public health threat for an estimated 44 million American women and men.

Given the clinical significance of osteoporosis, it is critical to accurately identify individuals who are at risk of fracture. Osteoporosis is currently defined by the World Health Organization (WHO) as a bone mineral density measurement by dual energy X-ray absorptiometry (DXA)—termed a t-score—that is 2.5 standard deviations below the normal level for sex-matched young individuals [2]. While DXA works reasonably well for predicting hip fractures, it is less successful at predicting vertebral fractures [3]. For example, bone mineral density alone has difficulty differentiating between patients with and without vertebral fractures [4]. Another recent study indicated that only 44% of women and 21% of men presenting with non-vertebral osteoporotic fractures had DXA t-scores in the osteoporotic range [5]. This suggests that over half of those individuals who eventually fracture are not classified as osteoporotic by WHO guidelines. These high-risk individuals often do not receive drug treatments, which have been shown to reduce fracture risk by ~50% [6-9]. Together, these findings have incited in the field of osteoporosis research the need to go beyond bone mineral density as the means of assessing fracture risk [10].

One major obstacle in improving vertebral fracture risk assessment is the incomplete nature of our understanding of the biomechanical mechanisms of vertebral strength and the etiology of vertebral fractures. Specifically, a number of fundamental questions remain unanswered. What are the relative roles of the various vertebral compartments in vertebral biomechanical behavior? Where do the highest stresses and strains occur in the vertebra and how well do the variations in these highly-stressed or highly-strained tissues explain variations in vertebral strength across individuals? What are the failure mechanisms in the vertebra and how do these failure mechanisms depend on an individual's bone morphology?

In addressing these issues, the goal of this dissertation is to enhance the current understanding of the biomechanical mechanisms of vertebral strength and the etiology of vertebral fractures. Understanding the biomechanical mechanisms is important for improving vertebral strength prediction and fracture risk assessment clinically; understanding fracture

etiology is important for elucidating the effects of aging and disease. The remainder of this chapter will establish a foundation in whole-vertebral biomechanics that will be useful in understanding the material presented in subsequent chapters of this dissertation. First, the structure and composition of bone will be briefly summarized, followed by detailed discussions of the anatomy and mechanical behavior of the human vertebra. Next, a short section will describe various measures of trabecular microarchitecture. The fifth section will address contemporary issues regarding finite element modeling of the vertebra. The final section contains an outline of the objectives and scope of this dissertation.

1.1 Structure and composition of bone[*]

Bone is a hierarchical composite material composed of structures that vary in size from a few nanometers to tens of millimeters (Figure 1-1). By weight, the constituent materials of bone are inorganic ceramic materials (primarily hydroxyapatite, 60%), organic materials (primarily type-I collagen, 30%), and water (10%). At the smallest size-scale, the hydroxyapatite crystals may resemble small plate-like structures (~5 *x* 15 *x* 40 nm). These crystals are surrounded by woven collagen fibrils (~30 nm in diameter *x* 300 nm in length). At the next size-scale (~10 μm), the mineralized collagen fibrils are arranged in one of two forms. In the first form, the fibrils randomly orient to form a structure often termed woven bone. In the second form, the fibrils assemble into sheets called lamellae, which then stack together in layers with alternating fiber angles between layers.

Lamellae are arranged in five different structures at the next size scale.

1. Trabecular bone, a highly porous structure (>60% porous in humans) is made of an organized lattice of lamellar packets. Trabecular bone occupies the ends of the long bones and the vertebral centrum; the trabecular lattice resembles an interconnected network of rod-like and plate-like struts with substantial variability across anatomic sites and species (Figure 1-2). Trabecular thickness is variable, but generally ranges between ~100-250 μm.
2. Osteonal or Haversian bone consists of 10-15 lamellae arranged in concentric cylinders (~200 μm in diameter *x* 2 mm in length) about a central Haversian canal. These canals contain blood vessels, capillaries, nerves, and bone cells. The substructure of the concentric lamellae is termed an osteon. Osteons are the primary discrete units of human cortical bone.
3. Primary lamellar bone is wrapped circumferentially in a 2-3 mm layer around the diaphysis of long bones such as the femur and tibia.
4. Woven bone is found in areas of rapid growth such as at locations of fracture.
5. Laminar bone consists of a series of concentric laminae (each laminae is ~0.1-0.2 mm thick) around a marrow cavity. Sandwiched between adjacent laminae is a two-dimensional network of blood vessels.

The underlying bone tissue that forms trabecular and cortical bone is very similar. Differences arise from the manner in which the two types of bone are remodeled. Remodeling in trabecular bone occurs at the free surfaces of the rods and plates, which is greater than on the

[*] Portions of this section were adapted in part from [11].

internal surfaces of the Haversian canals within cortical bone. As a result, trabecular bone is less mineralized than cortical bone. The details of trabecular and cortical morphology in the vertebra will be addressed in the next section.

Bone remodeling is crucial for skeletal adaptation. At the cellular level, this process is carefully orchestrated through the resorption of existing bone matrix by osteoclasts and the formation of newly mineralized material by osteoblasts. Continuous remodeling ensures the bone structure is most suited to the external loads being applied. Remodeling also results in constant fluctuations in local levels of tissue mineralization and in overall bone mass. Imbalance between the resorption and formation phases of the remodeling process due to aging and disease—such as osteoporosis—are thought to cause a net bone loss. Osteocytes are cells that reside in lacunae (5-8 μm in diameter) within and between lamellar packets. These cells are capable of sensing mechanical stimuli via primary cilia [12] and are thought to coordinate the remodeling process through gap junction-based signaling [13].

1.2 Anatomy of the vertebra*

The human spinal column is composed of thirty-three vertebrae separated by intervertebral discs. Each vertebra consists of four principal struc tural components: the trabecular centrum, the endplates, the cortical shell—all parts of the vertebral body (Figure 1-3)—and the posterior elements.

At the inferior and superior surfaces of the vertebra, the porous endplates support stresses imposed by the intervertebral discs and act as a nutrient pathway between the disc and the vertebra [15]. The microstructure of the endplates (~0.4-0.8 mm thick [16, 17]) more closely resembles that of condensed trabeculae than of Haversian cortical bone [17-19]. Endplate thickness depends on spinal level and position in the endplate [16, 20]: the endplates are thinner in the center than in the periphery [16] and at a given spinal level, superior endplates are also thinner than inferior endplates [20].

The cortical shell forms the periphery of the vertebral body. By weight, the thin, porous shell (0.25-0.4 mm thick [16, 17, 21, 22]) amounts to ~10-20% of the bone tissue in vertebral body [23]. Shell thickness varies transversely—it is thickest near the endplates and thinnest in the mid-transverse region [16].

The trabecular bone is located in the interior of the vertebral body. The volume fraction of trabeculae varies with location in the vertebral body [24-26] and with spinal level [27, 28]. Trabecular microarchitecture, which will be discussed in subsequent sections of this chapter, refers to the structure, interconnection, and spatial organization of the trabeculae. Vertebral trabecular bone has a highly porous (>80% porosity), rod-like architecture (Figure 1-2).

The posterior elements are boney processes that extend from the posterior aspect of the vertebral body. Two pairs of facet (apophyseal) joints connect adjacent vertebrae in the inferior

* Portions of this section were adapted in part from [14].

and superior directions. In the lower thoracic and lumbar spine, the facets resist transverse shear and restrict excessive motion in the torsion and extension [29].

1.3 Mechanical behavior of the vertebra*

Unlike osteoporotic hip fractures, which are attributable to a fall in approximately 90% of all cases [30, 31], many osteoporotic vertebral fractures result from non-traumatic loading conditions [32, 33]. This makes it difficult to diagnose vertebral fractures since they may initially be asymptomatic and often, do not present as sudden, discrete fractures [32]. Vertebral fractures are commonly grouped into three morphological cases: anterior wedge, biconcavity, and compression fractures [34](Figure 1-4). Anterior wedge fractures [34] and compression fractures [35] are the most common types of vertebral fractures. Understanding why and how failure occurs in the different compartments—endplates, cortical shell, trabecular bone—during an overload of the vertebra is a fundamental issue in diagnosing osteoporotic vertebral fractures, which remains a controversial topic [36].

Substantial changes occur to the vertebra with aging (Figure 1-5). Loss of bone density and deterioration in bone microarchitecture with age are thought to be the primary cause of decreases in vertebral strength [37]. One study estimates that vertebral strength decreases by about 12% per decade from ages 25-85 [38]. Aging is also accompanied by osteoarthritic changes around the intervertebral disc and endplates [39], including disc degeneration, and there are likely adaptive alterations of the bone within the vertebra in response to these changes [26]. While age accounts for about 60% of the variation in bone strength [38], individuals can exhibit much stronger or weaker bones than would be predicted by their age alone. Bone density can be thought of in a conceptually similar manner—even though density can account for much of the variation in bone strength, individual measures of strength can greatly exceed or fall short of the expected value at a given density. This issue underscores the importance of developing an improved understanding of the failure mechanisms in the vertebra and characterizing the relative structural contributions from the trabecular microarchitecture and the cortical shell.

The contribution of variations in trabecular microarchitecture to the failure mechanisms in the vertebra remains a source of much uncertainty. For example, trabecular buckling has long been proposed as one of the mechanisms by which small changes in density and architecture, *e.g.* thinning and fenestration of trabeculae, result in disproportionate changes in vertebral strength [40, 41]. Trabecular bending and buckling has been observed in isolated specimens of trabecular bone [42], and variations in trabecular microarchitecture parameters—indices that describe the physical characteristics of the trabeculae such as their thickness, separation, and connectivity—can explain variations in such large deformation-type failure mechanisms [43-45]. In the whole vertebra, however, the failure mechanisms are unclear, as is the dependence on trabecular microarchitecture. Given the clinical interest in using trabecular microarchitecture to supplement bone mineral density for fracture risk assessment [46, 47], determining the role of trabecular microarchitecture in whole-vertebral biomechanical behavior is critical.

* Portions of this section were adapted in part from [14].

The structural contribution of the cortical shell is also an important research topic. Recent advances in micro-CT imaging and high-resolution finite element modeling have provided a precise means for quantifying cortical-trabecular load sharing in the elderly spine [48, 49]. These studies predict that the cortical shell caries ~38-55% of the axial compressive load at the mid-transverse plane of the vertebra and substantially less (~11-26%) nearer to the endplates [49]. Perhaps even more striking is the structural contribution of the shell to whole-bone behavior: the stiffness of the shell alone is <10% of the stiffness of the intact vertebra, but removing the shell leads to >50% reduction in vertebral stiffness [48]. Experimental studies have found that the shell supports anywhere from 10% [50] to 75% [51] of the axial compressive load. Clearly, the cortical shell is an important load-bearing structure in the vertebra; however, the role of the shell in explaining the *variations* in vertebral strength across individuals as well as how its role compares to the role of trabecular microarchitecture are open questions.

Despite the endplates' functional role in transmitting loads between the intervertebral disc and the vertebra, the endplates remain an understudied anatomic region in the spine. The stresses along the endplates depend on the level of degeneration of the adjacent discs. A healthy disc has a gelatinous nucleus pulposis [52, 53], and applied compression concentrates load to the center of the endplates [54-57]. In contrast, a degenerated disc loses its fluid-like behavior [58, 59] and applied compression concentrates load to the ring apophysis and the cortical shell [56, 57, 60]. Endplate-disc interactions may even be an important determinant of vertebral strength. For example, a recent study which observed frequent endplate failures found that variations in disc properties were highly associated ($r^2 = 0.70$) with variations in vertebral strength [25], although the link between variations in disc properties and the mechanism of endplate or vertebral failure was unclear. The frequent involvement of the endplates in osteoporotic vertebral fractures [61-64] warrants further study of the mechanistic link between disc properties and the biomechanical behavior of the endplates.

1.4 Trabecular microarchitecture

The spatial arrangement and interconnection of individual trabeculae is termed trabecular microarchitecture. Several parameters have been developed to describe various aspects of trabecular microarchitecture. In this dissertation, the trabecular microarchitecture parameters are used as a tool for understanding the relationship between the structure of the trabecular bone and the behavior of the vertebra.

Microarchitecture parameters that will be used include: trabecular thickness (Tb.Th), trabecular separation (Tb.Sp), trabecular number (Tb.N), structural model index (SMI), connectivity density (Conn.D), and degree of anisotropy (DA). Tb.Th is defined as the average thickness of a trabecular object and Tb.Sp is defined as the average thickness of a pore space. Tb.N can be thought of as the average number of times per unit length that any random line drawn through the volume of interest intersects a trabecular object. SMI is used to quantify the structural appearance of trabecular bone by relating the convexity of the structure to a type of model [65]. Flat, plate-like structures have an SMI of zero and ideal cylindrical rods have an SMI of three. Conn.D is defined per unit volume and is related to the maximal number of branches that can be broken before a structure is separated into two parts [66]. Finally, DA quantifies the presence or absence of preferential alignment along a particular directional axis. A

perfectly isotropic structure has a DA of one and increasing values of DA represent increasing degrees of anisotropy. All of the microarchitecture measures presented in this dissertation will be evaluated using the three-dimensional distance transformation approach, *i.e.* the so-called "direct approach" [67]. This approach makes no *a priori* assumptions about the structure type of the trabeculae.

In the context of micro-CT-derived microarchitecture parameters, bone volume fraction (BV/TV) is often used to describe the apparent density of the bone. Bone volume fraction is the fraction of the total volume that is occupied by the trabecular hard tissue. As many of the microarchitecture parameters are highly correlated with bone volume fraction, it has generally been difficult to characterize microarchitecture in a manner that explains variations in bone strength not accounted for by variations in bone volume fraction. The effect of the correlations between microarchitecture parameters and bone volume fraction on vertebral strength will be addressed in this dissertation.

Microarchitecture analysis is often coupled with high-resolution finite element modeling of trabecular bone. Since tissue material properties and boundary conditions in the finite element models are prescribed explicitly, any predicted variations in apparent- or tissue-level mechanical behavior across models are attributed solely to variations in microarchitecture. In this dissertation, microarchitecture analysis will be coupled with high-resolution finite element modeling of the whole vertebra. The association between variations in specific aspects of the microarchitecture and the mechanical properties will be quantified using statistical regression techniques.

1.5 Finite element modeling of the vertebral body

Finite element analysis is a powerful computational tool for investigating the biomechanical behavior of bone. This technique allows investigators to perform "virtually real" experiments that have several advantages over gold-standard biomechanical tests. First, the technique is non-destructive, so the effects of variables such as boundary and loading conditions [44, 48, 68] or material properties [69-71] can be evaluated in controlled, repeated measures-type parameter studies. Second, the technique can provide detailed insight into stress and strain distributions within the vertebra [49, 72, 73] (Figure 1-6), whereas biomechanical testing only yields information about the apparent-level mechanical behavior (or at best, about local stresses and strains on the surface of the vertebra using strain gauges [74]). Perhaps the greatest benefit of finite element modeling in bone mechanics research lies in combining the technique with biomechanical testing in order to leverage the individual strengths of each approach. In this manner, for example, researchers have gained substantial insight into tissue-level mechanical properties [75, 76] and failure mechanisms [43].

This dissertation reports on the use of high-resolution finite element modeling of whole vertebral bodies. These finite element models are constructed from micro-CT images (30 μm spatial resolution) of vertebral bodies by converting each voxel in the images to an eight-node brick element [76]. Hence, the models implicitly capture the spatially heterogeneous microarchitecture, the thin cortical shell, and the porous endplates of the vertebra (Figure 1-3). By accurately capturing the physics of these microstructures, the models can be used to understand the micromechanics of the vertebral body and to resolve issues such as the effect of the cortical shell in obscuring the role of trabecular microarchitecture in whole-vertebral

behavior. In addition to addressing this issue, this dissertation also uses the high-resolution finite element models to elucidate the failure mechanisms in the trabecular bone, cortical shell, and endplates including how these failure mechanisms vary—both quantitatively and qualitatively—across individuals exhibiting a wide range of bone morphologies.

In contrast to continuum-level finite element models based on quantitative-CT images (1-3 mm spatial resolution) in which each element is assigned a different material property based on its CT-derived density [60, 77-82], high-resolution finite element models typically use homogeneous and isotropic material properties. This enables separation of the effects of variations in microarchitecture from the effects of variations in material properties. Additionally, apparent-level predictions of mechanical properties as well as tissue-level stress and strain distributions from high-resolution finite element models with homogeneous and isotropic material properties have correlated well with experimental measures providing some level of validation for this modeling approach [43, 83-87].

Computationally, high-resolution finite element modeling of the whole vertebra requires both state-of-the-art software and hardware. In the past, high-resolution finite element models of trabecular bone have traditionally been solved with the iterative, element-by-element (EBE) preconditioned conjugate gradient (PCG) method [73, 76, 83, 85]. This method is memory efficient and the work per iteration and per degree of freedom is constant. However, because the number of iterations required to reduce the residual by a constant amount using the EBE-PCG method rises dramatically as the problem size increases, this method is inefficient for solving larger problems, such as those involving the whole vertebra. The models of whole vertebrae typically contain on the order of 300 million degrees of freedom, and therefore, the analyses require more efficient solvers [88, 89] and substantial parallel computing capacity. By dividing the global finite element mesh into sub-domains and spreading the workload over thousands of processors that perform the computations in parallel, previously intractable problems can be solved in minutes. The work in this dissertation utilizes a highly-scalable, implicit finite element framework (*Olympus* [88]) implemented on some of the world's fastest and most advanced parallel supercomputers. In particular, the work utilizes implementations of *Olympus* on two supercomputing platforms: 1) an IBM SP4 machine with 2,048 processors and over 4 TB of memory (Datastar; San Diego Supercomputing Center, San Diego, CA USA); and 2) a Sun Constellation cluster with 62,976 processors and 123 TB of memory (Ranger; Texas Advanced Computing Center, Austin, TX USA).

In addition to their large size, high-resolution finite element models of whole vertebrae represent a significant computational challenge due to their numerical complexity. For example, performing fully nonlinear analysis involves both material and geometric nonlinearities. Material nonlinearities are necessary in order to capture the tension-compression strength asymmetry of the bone tissue [45, 86]. Geometric nonlinearities—which involve updating the stiffness matrix based on changes to the orientation of the structure—are required to capture the deformation mechanisms such as large-deformation bending and buckling [43, 90]. Due to the computational challenge of simulating these nonlinearities, past studies on whole vertebrae have focused only on *linear* analysis [48, 49, 72, 73]. However, recent advances in supercomputing technology combined with efficient solver algorithms [88] have finally made it possible to perform fully

nonlinear, high-resolution finite element analysis of whole vertebrae. A chapter of this dissertation is devoted to such analyses—the first of their kind for whole bones— and in particular, to understanding how the failure mechanisms in the human vertebra during an isolated overload depend on bone volume fraction and architecture.

1.6 Objectives and scope of the dissertation

The overall goal of this dissertation is to enhance the current understanding of the biomechanical mechanisms of vertebral strength and the etiology of vertebral fractures. The first objective is to investigate the role of trabecular microarchitecture in the variations in vertebral strength, stiffness, and failure mechanisms. In addition to identifying the microarchitectural characteristics of the trabecular bone that are the best "markers" of variations in whole-vertebral biomechanical behavior, these studies will also quantify possible interactions between the cortical and trabecular compartments. The second objective of this dissertation is to investigate the mechanisms of endplate failure.

The first study presented in this dissertation (Chapter two) examines the role of trabecular microarchitecture in whole-vertebral biomechanical behavior. Via a combined experimental and computational approach, this work also provides a direct assessment of the fidelity of the linearly elastic finite element models that are used to make biomechanical predictions in subsequent studies. While the role of trabecular microarchitecture has been studied extensively in isolated specimens of trabecular bone, *e.g.* cylinders and cubes, its role in whole-vertebral behavior has not been previously addressed due to the challenge of performing both the microarchitecture and biomechanical assays on the same vertebrae.

Once the combined experimental and computational approach for microarchitecture analysis of biomechanical behavior has been established, the combined approach will be used to study the effects of trabeculae in different orientations (Chapter three). This study also proposes a new microarchitecture parameter for assessing vertebral strength based on insight gained directly from the finite element models.

Chapter four determines the contribution of variations trabecular density and architecture to the tissue-level failure mechanisms in the vertebra. Owing to the numerical complexity of simulating both geometric and material nonlinearities in high-resolution finite element models of whole bones, characterizing the failure mechanisms in this manner represents a significant challenge in the field of computational bone mechanics. Indeed, the nonlinear, high-resolution finite element analyses in this chapter are the first of their kind for whole vertebrae.

Chapter five explores the mechanisms underlying the failure of the endplates. Vertebral fractures often involve failure of the endplates; however, the reason for this remains up in the air. Elucidating the mechanisms of endplate failure is important not only for improving our understanding of the etiology of vertebral fractures, but is critical for developing objective criteria to identify vertebral fractures as well.

Finally, Chapter six provides concluding remarks and suggests future directions of research.

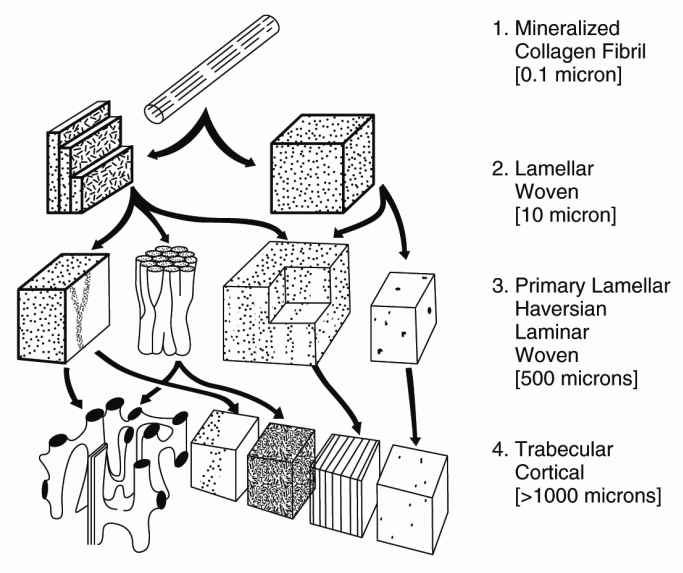

Figure 1-1: Hierarchical structures of bone from the sub-micron length scale to the millimeter length scale [11].

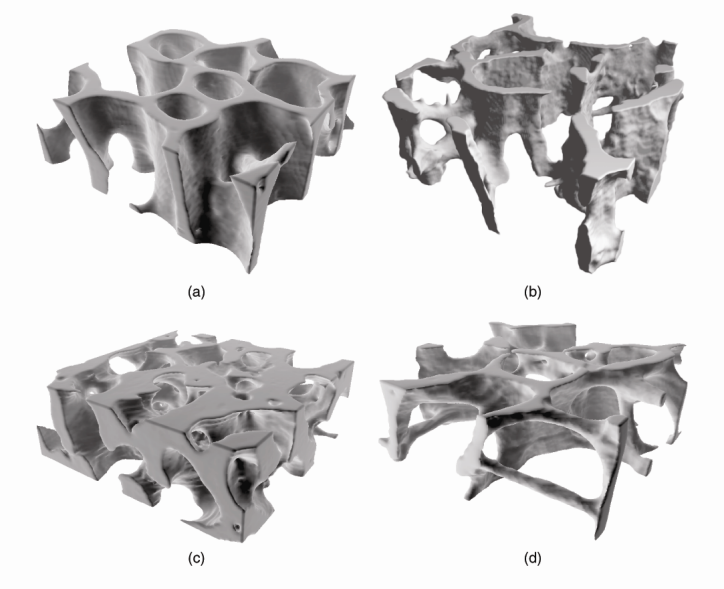

Figure 1-2: High-resolution renderings of trabecular bone from: a) bovine proximal tibia; b) human proximal tibia; c) human femoral neck; d) human vertebra [91].

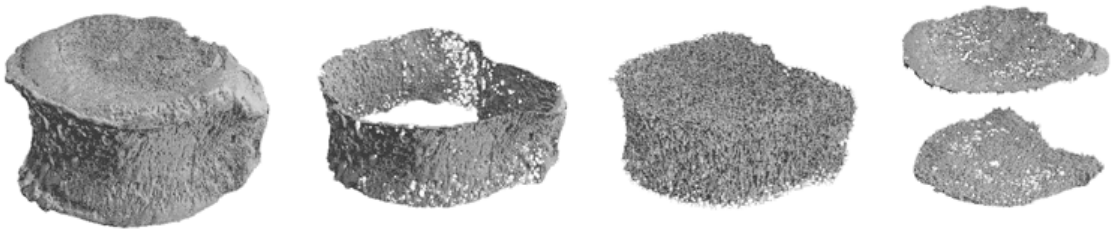

Figure 1-3: Vertebral body compartmentalized (from left to right) into the cortical shell, trabecular centrum, and endplates.

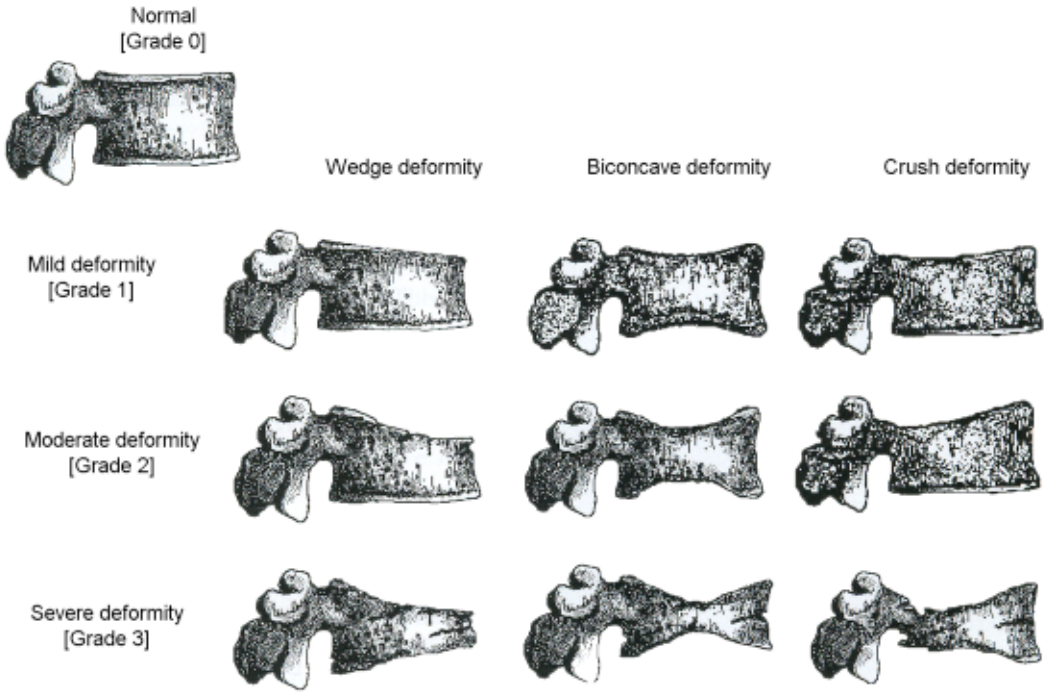

Figure 1-4: Vertebral body fracture classification and severity grading [34].

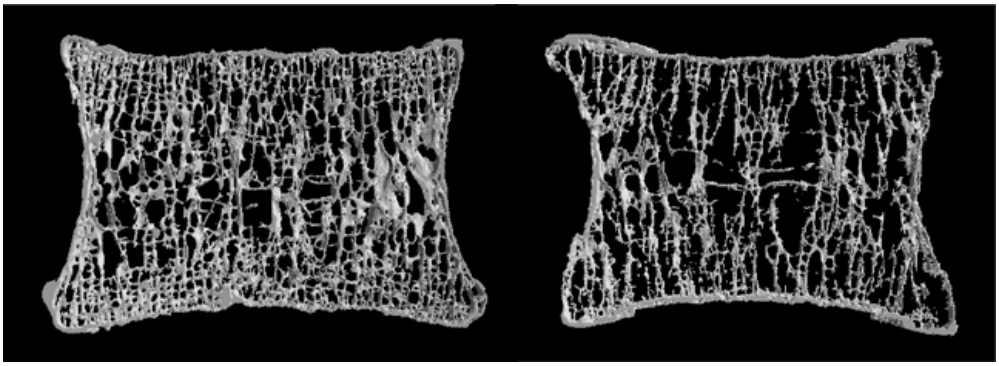

Figure 1-5: Mid-frontal sections of human T9 vertebrae from 53-year old (left) and 82-year old (right) donors. Aging and disease result in substantial loss of bone mass and deterioration in trabecular bone microarchitecture.

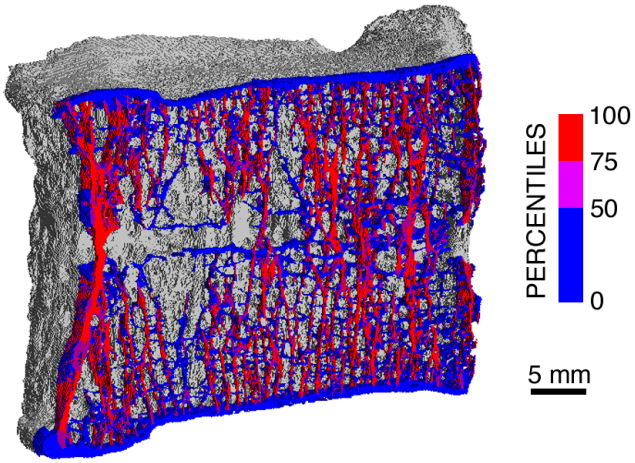

Figure 1-6: Mid-sagittal cutaway from a human T9 vertebral body showing the distribution of von Mises stress predicted by finite element analysis.

2. ROLE OF TRABECULAR MICROARCHITECTURE IN WHOLE-VERTEBRAL BODY BIOMECHANICAL BEHAVIOR

2.1 Introduction

The inability of DXA to accurately predict osteoporotic fractures [5] or fully account for decreases in fracture risk associated with anti-resorptive treatment [7, 9] has magnified clinical interest in parameters related to bone quality [92, 93]. Of particular interest is trabecular microarchitecture given its demonstrated role in the mechanical behavior of isolated specimens of trabecular bone [67, 83, 94, 95]. However, the influence of trabecular microarchitecture on whole-vertebral strength and stiffness is not well understood and may be obscured by potentially dominant morphological factors such as vertebral size, vertebral shape, overall bone mass, and the presence of the cortical shell. Understanding the relationships between microarchitectural and morphological indices and the biomechanical properties of the human vertebral body may therefore help elucidate the mechanisms by which trabecular microarchitecture contributes to vertebral fracture etiology.

Several factors contribute to a vertebra's biomechanical behavior, including bone mineral content and density [24, 28, 55, 96], cortical shell thickness [49], and geometric size and shape [27]. Despite the fact that the trabecular bone in the anterior and superior regions of the lumbar vertebra is less dense and connected than in the posterior and inferior regions [25, 97], it was recently reported that using measures of microarchitecture from a single region provided no additional predictive capability for strength compared to the use of whole-vertebral measures [25]. This raises questions about possible interaction effects between trabecular microarchitecture, the cortical shell—which has a substantial and complex load-bearing role in the human vertebra [49, 73, 98]—and vertebra size (reflected in part by overall bone mass) in terms of contributions to vertebral strength. It is possible, for example, that the role of trabecular microarchitecture in vertebral strength is influenced by the cortical shell or by bone mass.

The overall goal of this study was to investigate the role of trabecular microarchitecture in whole-vertebral biomechanical behavior, accounting also for such factors as vertebral mass, cortical shell morphology, and indeed the presence of the cortical shell itself. We addressed this issue using a combination of cadaver biomechanical testing, high-resolution micro-CT imaging, and micro-CT-based finite element modeling. Specifically, our objectives were to: (1) assess the individual effects of trabecular microarchitecture, cortical shell thickness, vertebral cross-sectional area, and bone mass on vertebral strength and stiffness; (2) determine the combined effects of these parameters on vertebral strength and stiffness; and (3) determine whether the physical presence of the shell alters the relation between trabecular microarchitecture and vertebral stiffness. This study is the first to relate the individual and combined effects of vertebral morphology, trabecular microarchitecture, cortical morphology, and the presence of the cortical shell to the biomechanical behavior in which all assays are performed on the same human vertebrae.

2.2 Methods

Fresh-frozen human spine segments were obtained from willed-body programs subject to exclusion of any donors having a documented history of metabolic bone disease, *e.g.*, metastatic cancer or hyper and hypothyroidism. Anterior-posterior and lateral view radiographs of accepted specimens were then examined to identify and exclude any T9 vertebrae showing evidence of pre-existing vertebral fractures or scoliosis. Twenty-two T9 vertebrae (n = 11 male; n = 11 female; age range: 53-97 years, mean ± SD = 81.5 ± 9.6 years) were thus obtained.

After removing the posterior elements, each isolated T9 vertebral body was micro-CT scanned using a 30 μm voxel size (Scanco 80; Scanco Medical AG, Brüttisellen, Switzerland) and a number of bone morphology and microarchitecture variables were measured from these scans. Bone mineral content (BMC) for each vertebra was estimated based on the measured bone volume and the assumption of constant tissue density (2.05 g/cc [99]), a technique that performs well when compared to DXA-derived BMC [100]. Model-independent trabecular microarchitectural parameters were measured for the largest internal cuboid region of trabecular bone, typically about 15 mm x 15 mm x 10 mm (Figure 2-1). The microarchitecture variables investigated were measured using the Scanco software and comprised: bone volume fraction (BV/TV), mean trabecular thickness (Tb.Th), mean trabecular number (Tb.N), mean trabecular separation (Tb.Sp), structural model index (SMI) [65], connectivity density (Conn.D) [66], and degree of anisotropy (DA).

To characterize biomechanical properties, destructive compressive tests were performed after micro-CT scanning for a subset of 16 vertebrae (n = 10 male; n = 6 female; age range: 53-97, 77.5 ± 10.1 years; the remaining six vertebrae were unavailable since they were used in a different type of biomechanical testing experiment). The specimens were cleared of soft tissues, placed between molds of polymethylmethacrylate bone cement to ensure plano-parallel ends [80, 101, 102], and tested at room temperature to failure in displacement control at either 0.50% strain/sec [102] or 0.06% strain/sec [77] following pre-conditioning [102]. Saline-soaked gauze was used to keep the samples moist throughout the experiments. Our main outcome parameter, vertebral strength (F_{ult}), was defined as the peak force achieved during the loading cycle [102], which occurred typically at a strain of about 1.8%. Vertebral stiffness was not measured because we did not use specimen-attached extensometers and thus machine compliance effects would confound the resulting deformation measures. Although the strength behavior of both cortical and trabecular bone depend on strain rate when strain rate is varied over many orders of magnitude [103, 104], the effect of strain rate is negligible in the range used here (p = 0.91; 0.1 *vs.* 1.0% strain/sec [103]). Thus, our data were not adjusted for any differences in applied strain rate.

In addition to this biomechanical testing, we performed finite element (FE) analysis on each of the n = 22 vertebral bodies to estimate vertebral compressive stiffness with and without the cortical shell. For each vertebra, two finite element models—one intact and one with the cortical shell virtually removed—were created using previously reported methods [48, 49, 72]. Briefly, the scans were region-averaged to 60 μm voxel size and segmented using a global threshold value. A custom algorithm (IDL 6.2; ITT Visual Information Solutions, Boulder, CO USA) using moving averages [48, 49] was used to identify the cortical shell. Each 60 μm cubic

voxel was then converted into an 8-noded element to create a finite element model of the entire vertebral body. Since the cortical shell is often described as condensed trabeculae [17-19], all cortical and trabecular bone elements in the models were assigned the same hard tissue properties (elastic modulus 18.5 GPa and Poisson's ratio of 0.3). Polymethylmethacrylate (elastic modulus 2.5 GPa and Poisson's ratio of 0.3 [105]) layers were added to the inferior and superior endplates of the vertebral body to mimic experiments. In order to determine how the presence of the shell influences the role of trabecular microarchitecture in vertebral biomechanical behavior, a second finite element model without the cortical shell was created for each specimen, and stiffness was computed for this model while keeping all other model inputs the same as in the intact model.

The resulting finite element models had up to 80 million elements and over 300 million degrees of freedom and required highly specialized software and hardware for analysis [88]. To simulate compressive loading, the superior surface of each model was displaced to 1.0% apparent level strain in the inferior-superior direction while the inferior surface was fixed to mimic experimental testing protocols. All analyses were run using custom code—including parallel mesh partitioner and algebraic multigrid solver [88]—on an IBM Power4 supercomputer (Datastar; San Diego Supercomputer Center, San Diego, CA USA), and required a maximum of 880 processors in parallel and 1800 GB of memory.

These analyses provided a number of outcome parameters. Vertebral stiffness (K_{intact}) was defined as the ratio of the reaction force generated at the inferior surface to the applied displacement. A similar calculation was used to define the stiffness of the trabecular compartment (K_{trab}) but using instead the results from the vertebra model without the shell. The contribution of the trabecular compartment to whole-vertebral stiffness, an indicator of load sharing between the cortical and trabecular bone, was quantified by the ratio K_{trab}/K_{intact}. The region-averaged 60 μm models were also used to calculate the average thickness of the cortical shell (Ct.Th) in the transverse region excluding the endplates [49] as well as a ratio of cortical shell mass to whole bone mass—cortical mass fraction (Ct.M). Minimum vertebral cross-sectional area (CSA) was determined using a moving average for 1-mm thick transverse slices.

The independent roles of trabecular microarchitecture, cortical shell thickness, and vertebral morphology in the biomechanical outcomes were quantified by the Pearson correlation coefficient. All explanatory variables were also correlated with each other to explore cross-correlation effects. The combined roles of trabecular microarchitecture, morphology and BMC in strength and stiffness were quantified using stepwise multiple linear regressions (JMP 7.0; SAS Institute Inc., Cary, NC USA), which sequentially add the most significant explanatory variable to the model until the unexplained variability in the dependent parameter cannot be reduced. To determine if the presence of the cortical shell alters the role of microarchitecture, stiffness-architecture relationships were determined using intact and trabecular stiffness as the outcome. The statistically significant intact and trabecular stiffness-architecture relationships were then compared using a *t*-test on the regression slopes. All regressions and tests were taken as significant at $p < 0.05$.

2.3 Results

The average value of bone volume fraction was less than 10% (Table 2-1), indicating the low-density nature of the vertebrae analyzed. Consistent with this, strength values (1420-6570 N) were typical of an elderly cohort with low bone mass [55].

Of all measured explanatory variables, BMC (r = 0.76) and SMI (r = -0.76) displayed the highest associations with vertebral strength, whereas BMC was most highly associated with vertebral stiffness (r = 0.90, Table 2-2). Overall, the remaining trabecular microarchitectural parameters displayed modest correlations with either vertebral strength or stiffness ($|r| = 0.21$-0.66), with significant correlations only occurring for SMI and BV/TV. As expected from previous studies [79], finite element-computed whole-vertebral stiffness and compression test-measured vertebral strength were highly correlated (r = 0.87). Vertebral strength and stiffness were weakly correlated with donor age (r = -0.50 and r = -0.66, respectively) but not with donor body mass.

Results from the multiple regression analyses indicated that trabecular microarchitecture was strongly associated with vertebral strength and stiffness, but its role was mediated by BMC (Figure 2-2). Combined measures of trabecular microarchitecture (SMI and Tb.Th)—when considered without data on BMC and cortical morphology—could explain an appreciable degree of variability in vertebral strength ($R^2 = 0.76$) and stiffness ($R^2 = 0.62$). However, when BMC was added to the model, the architecture variables in the multiple regression model changed (strength: DA and BV/TV; stiffness: DA) and the degree of correlation increased (strength and stiffness: $R^2 = 0.85$). Scatter plots of the regression models with BMC alone and with BMC plus microarchitecture as predictors of vertebral strength (Figure 2-3) and a comparison between the changes in the residuals for the weaker half ($n = 8$) versus the stronger half ($n = 8$) of the specimens revealed significantly greater reductions for the weaker group (Wilcoxon rank-sum test, $p = 0.04$). This indicates that including microarchitecture parameters in the model had a greater effect on the low-strength specimens. Variations in cortical morphology were not associated with vertebral strength after accounting for either microarchitecture or BMC.

One-way correlations between the explanatory variables demonstrated a number of moderately strong cross-correlation effects (Table 2-3). For example, BMC was correlated ($|r| > \sim 0.5$) with the structure and density of trabecular bone (SMI and BV/TV, respectively), cortical shell morphology (Ct.Th and Ct.M), and vertebral size (CSA).

Relationships between each of the microarchitecture parameters and vertebral stiffness with the shell removed were similar to those with intact vertebral stiffness (*t*-test on regression slopes, $p = 0.09$-0.63), indicating that the physical presence of the cortical shell did not alter the relationships between trabecular microarchitecture and vertebral stiffness. The unique mechanical contribution of the trabecular bone, K_{trab}/K_{intact}, varied from 36% to 73% of the intact vertebral stiffness and was most significantly associated with the relative amounts of cortical and trabecular bone (Ct.M, r = -0.85). Of the microarchitecture parameters, there was an association between the stiffness contribution of the trabecular compartment and the plate-like nature of the trabeculae (SMI, r = -0.54).

2.4 Discussion

Taken together, these results show that trabecular microarchitecture was highly associated with vertebral strength and that its role was mediated by bone mass but not by cross-sectional area or the cortical shell. This mediation effect was due in part to significant cross-correlations between bone mass and trabecular microarchitecture. As a result of these cross-correlation effects, different microarchitecture parameters were associated with measured vertebral strength when included in a multiple regression model with bone mass (DA and BV/TV) than when included in a model without bone mass (SMI and Tb.Th). Bone volume fraction is related to porosity (= 1–BV/TV) and can be considered a surrogate of volumetric bone density rather than a strict measure of microarchitecture. Thus, while SMI and Tb.Th together appear to be the most important microarchitecture parameters when bone mass and trabecular density are not available, the degree of anisotropy appears to be the most important microarchitecture parameter when bone mass and density data are available. Further, our findings suggest that the role of microarchitecture may be more important in low-strength specimens.

One unique feature of this study was our use of the finite element modeling technique to virtually remove the cortical shell—a task that would have been difficult to perform experimentally—in order to test whether its physical presence alters the role of trabecular microarchitecture on whole-vertebral stiffness. This provided mechanistic insight into the multiple regression analyses. We also performed all assays on the same specimens, thereby eliminating scatter due to the use of neighboring vertebrae or peripheral sites for microarchitecture and biomechanical analyses. In addition, model-independent microarchitectural parameters were determined from micro-CT scans at 30 μm resolution to reduce partial volume effects on measurement accuracy [106]. In terms of external validity, this elderly cohort spanned a range of equivalent QCT-BMD values for trabecular bone (determined using a linear relationship between apparent density and QCT-BMD [107]) both above (n = 11) and below (n = 11) a reported clinical fracture threshold of 110 mg/cc [108], and thus represented a population at risk for vertebral fracture.

The most important limitation of this study was the modest sample size, which may prevent the extension of our findings to a wider range of bone phenotypes, including younger individuals with higher bone volume fractions. Additionally, the loading conditions used for the biomechanical assays were chosen to provide controlled boundary conditions common in laboratory cadaver testing, but as a result were not fully representative of *in vivo* loading. Under more physiological loading conditions, the endplates should experience larger strains than those observed here [54, 72], and thus it is not clear how our results would change if the vertebrae were compressed via intervertebral discs. However, a previous study [25] on functional spine units (which allowed loading via a disc) reported only a moderate correlation (r^2 = 0.38; p = 0.003) between yield strength and endplate thickness. Moreover, since the cortical shell is loaded less during compression through the disc, the role of the shell in vertebral strength, including any tendency to obscure trabecular contributions, may be even smaller than reported here. Associated with this issue is the effect of any added bending moment—possibly arising due to forward flexion—on the relative contributions of the trabecular and cortical compartments compared to the case of uniform compression. Though *in vivo* loads on the vertebral body during

flexed postures are not well understood, preliminary studies suggest peripheral bone has a greater role under bending loads [109] and that less optimal stress transfer may occur in osteoporotic trabecular bone [73]. Further investigation is required to address this issue.

A more technical caveat of our approach is that the absence of stiffness data from the mechanical tests prevented us from correlating FE predictions with experimental results. Unlike in our models, stiffness is difficult to measure in the experiments for several reasons. First, the force-deformation curve is not linear; therefore, experimental measures of stiffness are highly sensitive to the region of the curve analyzed. Second, due to machine compliance and the possible presence of soft tissue or gaps between the PMMA and endplates, stiffness measured from crosshead displacement is not reflective of the actual stiffness of the vertebra—a challenge since the FE models contain an idealized interface between the PMMA and bone. However, the high correlation between FE-predicted and experimentally measured stiffness [83] found previously for trabecular cores lends support to the validity of our models. Additionally, element size was determined from a numerical convergence analysis [49]. Since we applied the same linear modeling technique to all specimens, relative predictions of stiffness as well as the role of microarchitecture should be robust.

One clinical limitation is that a lack of DXA or QCT data for this cohort did not allow us to compare against those modalities. At the time of these scans, we did not have a standard calibration of the tissue density detected by the micro-CT scanner. However, a recent study comparing DXA-derived BMC with micro-CT estimates using the assumption of constant tissue density revealed excellent agreement ($r^2 = 0.96$, slope of 1) between these two techniques [100]. Moreover, the coefficient of variation in mean tissue mineral density for human trabecular bone is <2.5% [110] and thus, the error in BMC estimates associated with our assumption of constant tissue density should not be appreciable. Since we did not have DXA scans, we have no information on the role of microarchitecture in the presence of DXA-derived areal BMD data for the spine. Clinically, such BMD data would likely be combined with trabecular microarchitecture measurements from the spine or from peripheral sites, both at lower resolutions. Our findings are consistent with results from a previous study that found trabecular microarchitecture parameters in the spine, particularly SMI and BV/TV, were highly indicative of vertebral fracture risk [46]. At peripheral sites, trabecular microarchitecture is weakly correlated with that of the spine [111], and clinical studies using architecture from peripheral sites to differentiate vertebral fracture patients from non-fracture controls have had mixed success [47, 82]. Additional research is required to elucidate the role of microarchitecture from peripheral sites in vertebral fracture risk.

The results of this study are consistent with and complementary to previous studies on the role of microarchitecture in vertebral strength [25, 100, 112], and taken together suggest that improvements in vertebral strength prediction are best achieved through considering the trabecular microarchitecture of the vertebra of interest. One-way strength-architecture relationships were in close agreement with those found by others [25], indicating that a vertebra's strength does indeed depend on its trabecular microarchitecture. Yet, the role of trabecular microarchitecture was only marginal in the strength of a neighboring vertebra [112]. The current results can thus be thought of as a best-case scenario for the use of microarchitecture

measures to predict vertebral strength. Volume fraction accounts for the fact that larger vertebrae are less dense than smaller specimens with the same BMC; after bone size and quantity effects, the remaining differences in vertebral strength were most significantly associated with variations in the degree of trabecular anisotropy. Pooled results from a recent monkey study showed a comparable increase (from 67% to 88%) in prediction of measured strength by including Tb.Sp, SMI, and bone surface-to-volume ratio with BMC of the same specimens [100]. Bone volume fractions were approximately ~26-32% in that study. It remains to be seen whether the microarchitecture parameters most associated with human vertebral strength after accounting for bone mass are the same for both low- and high-density vertebrae.

Our results demonstrated that the physical presence of the shell does not appear to change the role of trabecular microarchitecture in vertebral stiffness. One implication of this unexpected result is that the insight gained from studying the effects of microarchitecture in isolated specimens of trabecular bone may extend to whole-vertebral behavior. Along with the stiffness-architecture relationships, strength-architecture relationships may too be unaffected by the presence of the shell since microarchitecture and cortical morphology had similar independent effects on both vertebral stiffness and strength. Another interesting finding was that cortical morphology was not associated with vertebral strength in multiple regression. One hypothesis is that the failure behavior of the vertebra is more sensitive to differences in trabecular microarchitecture that reflect the bone's susceptibility to buckling (*e.g.* Tb.Th and SMI) [41] rather than to differences in cortical shell morphology. Given the shell's substantial contribution to vertebral strength [51, 113] and stiffness [48, 49, 73] and that a recent clinical study using finite element analysis of QCT scans indicated a potentially important role of the peripheral bone on vertebral fracture risk [82], further research is recommended into the independent role of the cortical shell for vertebral strength prediction and clinical fracture risk assessment. The current data are not inconsistent with those findings; instead, they suggest that the roles of the cortical shell and trabecular microarchitecture are largely independent. We also note that the plate-like nature of the trabeculae was individually predictive of the stiffness contribution of the trabecular compartment (K_{trab}/K_{intact}), but that the effect was secondary compared to the relative mass of the cortical and trabecular bone. While this supports the argument that compressive load sharing may primarily involve vertically aligned bone tissue [48], additional research is required to understand the contributions of horizontal and vertical trabeculae to whole-vertebral biomechanical behavior [114].

In summary, our findings demonstrate that trabecular microarchitecture was highly associated with whole-vertebral biomechanical behavior and that its role was mediated by BMC but not by vertebral cross-sectional area or the cortical shell. Further, it appears that the role of trabecular microarchitecture, when considered in conjunction with information on bone mass and density, was more accentuated in low-strength vertebrae and involves mostly the degree of anisotropy.

Table 2-1: Donor, whole bone morphometry, cortical shell, trabecular microarchitecture, and biomechanical data for the 22 human T9 vertebral bodies included in this study.

	Mean	SD	CV* (%)	Range
Donor				
Age (yr)	81.5	9.6	11.8	53 – 97
Body mass (kg)	59.9	12.2	20.3	38.6 – 86.4
Whole bone morphology				
BMC (g)	8.16	3.01	36.9	3.7 – 13.5
CSA (cm^2)	8.49	1.59	18.7	5.8 – 11.3
Cortical shell				
Ct.Th (mm)	0.38	0.09	24.5	0.25 – 0.54
Ct.M (%)	14.5	3.3	22.9	8.9 – 21.5
Trabecular microarchitecture				
BV/TV (%)	9.8	1.8	18.9	7.2 – 14.1
Tb.N (mm^{-1})	0.99	0.10	10.3	0.78 – 1.14
Tb.Sp (mm)	0.98	0.11	11.5	0.82 – 1.21
Tb.Th (mm)	0.16	0.02	13.8	0.12 – 0.22
DA	1.42	0.08	5.7	1.27 – 1.60
Conn.D (mm^{-3})	3.02	0.80	26.6	1.16 – 4.48
SMI	2.19	0.30	13.6	1.34 – 2.72
Biomechanical properties				
Vertebral strength, F_{ult} (N) **	3250	1420	43.7	1420 – 6570
Vertebral stiffness, K_{intact} (kN/mm)	44.9	17.6	39.2	19.4 – 79.6
Trabecular stiffness, K_{trab} (kN/mm)	26.4	13.7	51.9	8.4 – 57.1
K_{trab}/K_{intact} (%)	56.6	10.8	19.1	35.7 – 73.2

* CV = SD/mean; SD = standard deviation
** Vertebral strength measured for 16 vertebrae

Table 2-2: Independent role (Pearson's correlation coefficient, r) of trabecular microarchitecture, cortical shell thickness, and vertebral morphology on biomechanical properties (n = 22 vertebral bodies, unless otherwise noted).

	BMC	CSA	Ct.Th	Ct.M	BV/TV	Tb.N	Tb.Sp	Tb.Th	DA	Conn.D	SMI
F_{ult}*	0.76[c]	0.48	0.50[a]	-0.45	0.66[b]	-0.28	0.21	0.31	0.46	-0.35	-0.76[c]
K_{intact}	0.90[c]	0.66[c]	0.66[c]	-0.49[a]	0.61[b]	-0.36	0.28	0.39	0.35	-0.38	-0.67[c]
K_{trab}	0.87[c]	0.69[c]	0.46[a]	-0.64[b]	0.62[b]	-0.31	0.24	0.33	0.35	-0.31	-0.73[c]
K_{trab}/K_{intact}	0.53[a]	0.50[a]	-0.10	-0.85[c]	0.40	-0.02	< 0.01	0.01	0.13	0.07	-0.54[b]

[a] $p < 0.05$
[b] $p < 0.01$
[c] $p < 0.001$
* Vertebral strength measured for 16 vertebral bodies

Table 2-3: Pearson's correlation coefficient (r) between BMC, trabecular microarchitecture, and morphology parameters as measured by micro-CT (n = 22 vertebral bodies).

	BMC	CSA	Ct.Th	Ct.M	BV/TV	Tb.N	Tb.Sp	Tb.Th	DA	Conn.D
BMC	-									
CSA	0.83[c]	-								
Ct.Th	0.66[c]	0.33	-							
Ct.M	-0.48[a]	-0.44[a]	0.16	-						
BV/TV	0.58[b]	0.31[a]	0.50[a]	-0.17	-					
Tb.N	-0.23	-0.34	-0.10	0.08	0.28	-				
Tb.Sp	0.19	0.34	0.06	-0.06	-0.37	-0.98[c]	-			
Tb.Th	0.30	0.29	0.28	0.07	0.29	-0.52[a]	0.45[a]	-		
DA	0.18	0.06	0.08	-0.24	-0.05	-0.69[c]	0.65[c]	0.45[a]	-	
Conn.D	-0.26	-0.32	-0.21	< 0.01	0.10	0.91[c]	-0.85[c]	-0.71[c]	-0.76[c]	-
SMI	-0.65[b]	-0.47[a]	-0.42	0.34	-0.69[c]	0.11	-0.08	0.04	-0.19	0.08

[a] $p < 0.05$
[b] $p < 0.01$
[c] $p < 0.001$

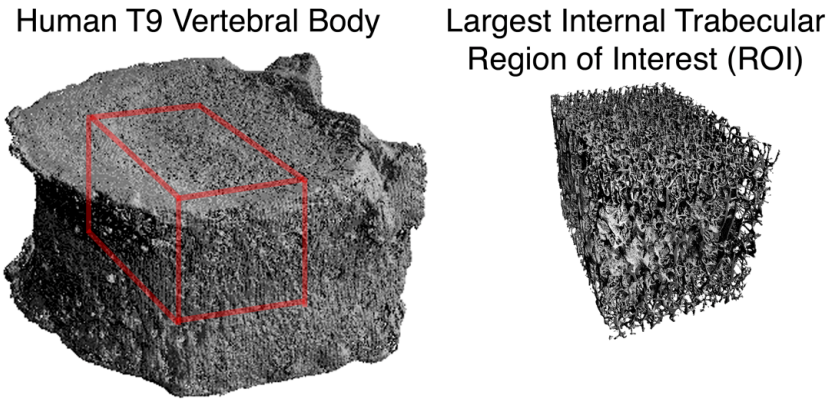

Figure 2-1: Example micro-CT rendering of a human T9 vertebral body (left) with largest internal cuboid of trabecular bone isolated for microarchitectural analysis (right).

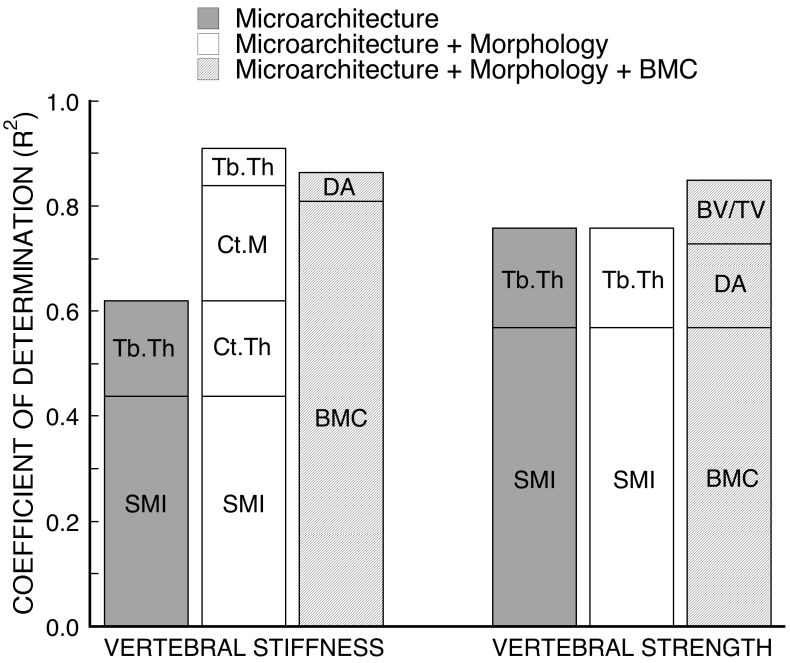

Figure 2-2: R^2 values for combined contributions of microarchitecture, morphology, and BMC in stepwise multiple regression models for FE-predicted vertebral stiffness (n = 22 vertebral bodies) and experimentally measured vertebral strength (n = 16 vertebral bodies). Microarchitecture considers all: BV/TV, Tb.N, Tb.Sp, Tb.Th, DA, Conn.D, and SMI. Morphology considers all: CSA, Ct.Th, and Ct.M.

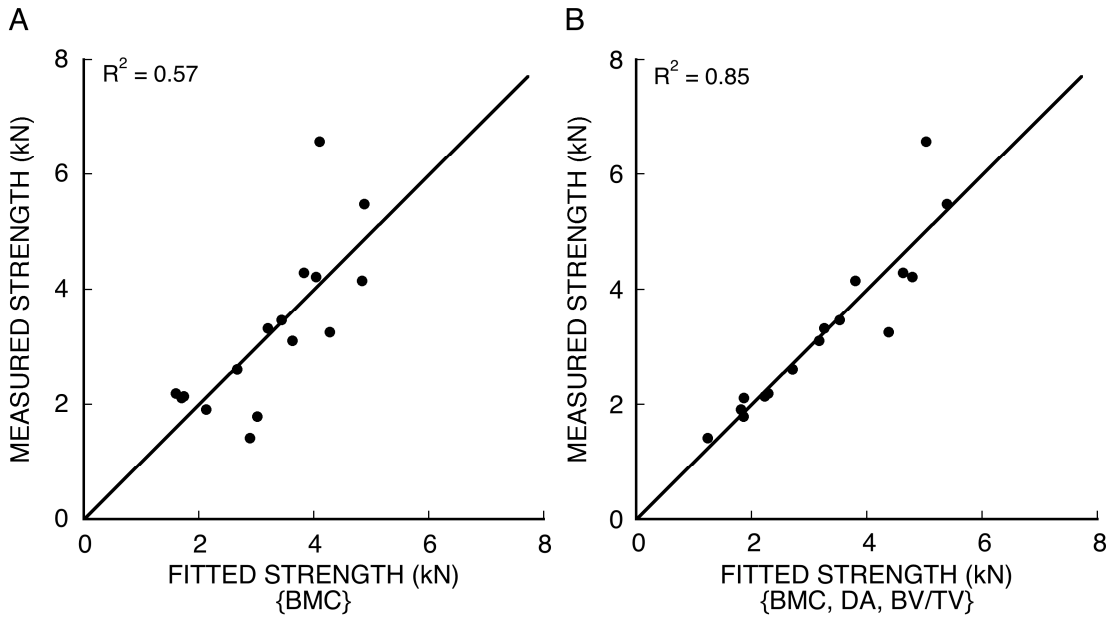

Figure 2-3: Fitted *vs.* measured vertebral strength. (A) BMC as a single predictor of strength (Strength = BMC*376 – 196). (B) BMC, DA, and BV/TV as predictors of strength (Strength = BMC*244 + DA*7660 + BV/TV*29700 – 12900).

3. INFLUENCE OF VERTICAL TRABECULAE ON THE COMPRESSIVE STRENGTH OF THE HUMAN VERTEBRA

3.1 Introduction

Osteoporosis decreases vertebral strength due to loss of bone mass and deterioration of bone microarchitecture. Osteoporosis also increases the anisotropy of the trabecular structure [115, 116] since more horizontal trabecular bone is lost than vertical trabecular bone [117]. The relative role of vertical versus horizontal trabecular bone on vertebral strength remains poorly understood and may provide new insight into the etiology of age- and disease-related vertebral fractures and could ultimately lead to improved prediction of vertebral strength and assessment of fracture risk. Previous work on isolated specimens of trabecular bone found that the bone volume fraction of vertical trabeculae better predicted overall mechanical behavior than did the bone volume fraction (BV/TV) of the entire specimen [118]; vertical trabeculae also failed in the greatest number [119]. However, extrapolation of those findings to the whole vertebral body is not obvious because the biomechanical behavior of the whole vertebra has a substantial and complex contribution from the cortical shell [48, 49, 51, 73, 98, 113], which could alter the effect of vertical trabeculae. Based on our previous findings that the roles of the cortical shell and trabecular microarchitecture—such as bone volume fraction—may be largely independent [23], we hypothesized that vertebral strength is better explained by the bone volume fraction of the vertical trabeculae than by the bone volume fraction of all trabeculae, and that the cortical shell does not alter the effect of vertical trabeculae on the biomechanical behavior of the vertebra.

3.2 Methods

Sixteen whole thoracic ninth (T9) vertebrae were obtained fresh-frozen from human cadaver spines (age = 77.5 ± 10.1, 53-97 years; n = 10 male, n = 6 female) with no history of metabolic bone disorders. As described elsewhere in more detail [23], the posterior elements were removed and each isolated vertebral body was micro-CT scanned with a 30 μm voxel size (Scanco 80; Scanco Medical AG, Brüttisellen, Switzerland). The scans were coarsened to 60 μm voxel size and the hard tissue and marrow were segmented using a global threshold value (Scanco). The bone tissue in the trabecular compartment was then digitally isolated from the cortical shell and endplates using a custom script (IDL 6.2; ITT Visualization Information Solutions, Boulder, CO USA) described in detail elsewhere [48, 72]. Briefly, the script uses a moving average of the thickness of the cortical shell and of the endplates to account for the thin and porous nature of these structures and to determine the boundary between these structures and any adjacent trabeculae.

Morphological analyses were performed to classify the orientation of trabeculae in the trabecular compartment. Individual trabeculae were identified using the Individual Trabeculae Segmentation (ITS) technique [118] and classified by orientation with respect to the superior-inferior anatomical axis: vertical (0-30°), oblique (31-60°), or horizontal (61-90°). We evaluated the following orientation-related morphology parameters for the trabecular compartment: bone volume fraction (BV/TV); bone volume fraction of vertical trabeculae (vBV/TV); bone volume fraction of oblique trabeculae (oBV/TV); bone volume fraction of horizontal trabeculae (hBV/TV); vertical tissue fraction (vBV/BV), the volume of vertical trabeculae divided by the volume of all trabeculae; oblique tissue fraction (oBV/BV), the volume of oblique trabeculae

divided by the volume of all trabeculae; and horizontal tissue fraction (hBV/BV), the volume of horizontal trabeculae divided by volume of all trabeculae. We also evaluated two variants of the vertical tissue fraction: $vBV/BV_{VERTEBRA}$, the volume of vertical trabeculae divided by the total volume of bone tissue in the vertebral body, *i.e.* trabecular bone + cortical shell + endplates; and $vBV_{VERTEBRA}/BV_{VERTEBRA}$, the volume of vertical bone tissue in the vertebral body, *i.e.* vertical trabeculae + cortical shell, divided by the total volume of bone tissue in the vertebral body.

To characterize the biomechanical properties of the vertebral bodies, destructive compression testing was performed after micro-CT scanning. Details of the biomechanical tests are described elsewhere in more detail [23, 77, 102]. Briefly, these experiments were conducted using a screw-driven load frame with a lockable ball joint to allow the top platen of the load frame to rest flat on the vertebrae during compression. The vertebrae were first placed between PMMA endcaps to ensure plano-parallel ends [80, 101]. The compression tests were performed in displacement control at a slow strain rate (~0.05-0.5% strain/s) after cyclic preconditioning [23]. Vertebral strength, F_{ult}, was defined as the peak force achieved during the loading cycle.

To identify the load-bearing tissues and to examine the interaction between the cortical shell and the trabeculae in each orientation, we performed high-resolution finite element analysis. Two finite element models—one model of each intact vertebra and one model of each vertebra with the cortical shell virtually removed—were created from the coarsened micro-CT scans [23, 72]. Each 60 μm cubic voxel in the scans was converted into an eight-noded brick element to create a finite element model of the entire vertebral body. Element size was chosen based on a numerical convergence study [72]. Linear finite element analysis was conducted for each model to 1% apparent compressive strain via simulated layers of polymethylmethacrylate (PMMA; elastic modulus 2.5 GPa and Poisson's ratio of 0.3 [105]) augmented to the inferior and superior endplates. All bone elements were assigned the same homogeneous and isotropic hard tissue material properties: elastic modulus 10 GPa [68], Poisson's ratio of 0.3. To determine the effect of the cortical shell, a second finite element model for each vertebra with the cortical shell removed was analyzed while keeping all other model inputs unchanged. Models contained 25-80 million elements. A highly scalable, implicit parallel finite element framework (*Olympus* [88]) was used for all analyses. These analyses were performed on an IBM Power4 supercomputer (Datastar; San Diego Supercomputer Center, San Diego, CA USA) and required up to 880 processors in parallel and 1800 GB of memory.

A number of outcomes from the finite element analyses were used to characterize the biomechanical behavior of the vertebral bodies. Vertebral stiffness of the intact vertebra (K_{intact}) and of the trabecular compartment (K_{trab}) were defined as the ratio of the reaction force to the applied displacement in the models with and without the cortical shell, respectively. Stress distributions in the models were used to identify the major load-bearing tissues in the vertebrae. These load-bearing tissues were defined as the elements having von Mises stress above the 75^{th} percentile in each model [120]. Varying the cutoff between the 75^{th}-90^{th} percentiles did not alter our conclusions.

The independent effects of the orientation-related morphology parameters on measured vertebral strength and finite element-predicted vertebral stiffness were assessed with the Pearson

correlation coefficient. To quantify the interaction between the cortical shell and the trabeculae in each orientation, relationships between stiffness and bone volume fraction were determined with intact stiffness and trabecular stiffness as the outcome. The statistically significant relationships were then compared using paired *t*-tests on the regression slopes and on the predicted residuals. The percentage of load-bearing tissue was compared across orientations using paired *t*-tests with Bonferroni adjustments for multiple comparisons. Multiple linear regression analysis was also used to investigate the combined roles of bone volume fraction and vertical tissue fraction in vertebral strength. All statistical tests (JMP 7.0; SAS Institute Inc., Cary, NC USA) were taken as significant at $p < 0.05$.

3.3 Results

Over half of the trabecular tissue was vertically oriented, more than twice the proportion of trabecular tissue that was either obliquely or horizontally oriented (Table 3-1). Due to the highly porous nature of the cohort (BV/TV = 14% ± 3%; mean ± SD), the bone volume fraction of vertical trabeculae (vBV/TV) ranged from just 4% to 11%.

The variation in both experiment-measured vertebral strength and finite element-predicted vertebral stiffness was most associated with the bone volume fraction of vertical trabeculae (Table 3-2). Compared with the bone volume fraction of all trabeculae, the bone volume fraction of vertical trabeculae accounted for substantially more of the variation in vertebral strength ($r^2 = 0.83$ *vs.* $r^2 = 0.59$, Figure 3-1) and had significantly lower residuals ($p < 0.005$ paired *t*-test on residuals, Figure 3-1). The bone volume fractions of oblique and horizontal trabeculae were not associated with vertebral strength and were weakly associated with vertebral stiffness. As expected, the bone volume fraction of vertical, oblique, and horizontal trabeculae were each correlated with total bone volume fraction ($r^2 = 0.90$, $r^2 = 0.80$, $r^2 = 0.51$, respectively).

After accounting for the variation in total bone volume fraction (BV/TV), the vertical trabeculae remained most strongly associated with vertebral strength by way of variations in vertical tissue fraction (vBV/BV: $r^2 = 0.81$, Table 3-2, Figure 3-2). Expressing the vertical trabeculae as a fraction of all of the bone tissue in the vertebral body worsened the correlation ($vBV/BV_{VERTEBRA}$: $r^2 = 0.56$, $p < 0.001$), as did including the cortical shell in the measure of vertically-oriented bone tissue ($vBV_{VERTEBRA}/BV_{VERTEBRA}$: $r^2 = 0.17$, $p = 0.12$). The vertical tissue fraction (vBV/BV) was only weakly correlated with total bone volume fraction (BV/TV: $r^2 = 0.28$; $p = 0.04$). In a multiple linear regression model with vertebral strength as the outcome, both the vertical tissue fraction (vBV/BV; $p < 0.0001$) and total bone volume fraction (BV/TV; $p < 0.0005$) were significant predictors (BV/TV alone: $r^2 = 0.59$; BV/TV and vBV/BV: $R^2 = 0.93$).

Results from the finite element models revealed that the physical presence of the cortical shell did not appreciably alter the degree of association between the bone volume fraction of vertical trabeculae and vertebral stiffness (Figure 3-3). Without the shell, the vertebral bodies were less stiff (downward shift in the regression data), but the interaction between the cortical shell and the bone volume fraction of vertical trabeculae varied little across individuals (no difference in residuals: $p = 0.92$; similar regression slopes; $p = 0.07$). Similarly, removing the shell had no significant effect on the relationship between the bone volume fraction of oblique trabeculae and vertebral stiffness (no difference in residuals: $p = 0.23$; no difference in regression

slopes: $p = 0.50$). The bone volume fraction of horizontal trabeculae was not significantly associated with the stiffness of the vertebra without the shell.

The stress distributions from the finite element models revealed that the major load paths in the vertebrae were vertically oriented (Figure 3-4). Of the tissue that was stressed in the 75th percentile, 41.2 ± 6.3% was composed of the vertical trabecular bone and 27.0 ± 5.6% was composed of the cortical shell. By comparison, significantly less of the tissue stressed in the 75th percentile resided in the oblique (10.4 ± 1.8%; $p < 0.0001$) and horizontal trabeculae (8.6 ± 2.2%; $p < 0.0001$). Removing the cortical shell did not alter the vertical nature of the load paths (Figure 3-4); as expected, it mainly resulted in unloading of the peripheral trabeculae [48].

3.4 Discussion

These results confirmed our hypothesis, demonstrating that variation in vertebral strength across individuals was primarily due to variations in the bone volume fraction of vertical trabeculae. This is because the major load paths in the vertebrae were parallel columns of vertically-oriented bone—the vertical trabeculae and the cortical shell. Whereas variations in the amount of vertical trabeculae had an important role in vertebral strength, variations in the amount of cortical tissue had a minor role [23]. Moreover, the cortical shell did not alter the association between the bone volume fraction of vertical trabeculae and vertebral stiffness. As with many microarchitecture parameters [23, 121], the bone volume fraction of vertical trabeculae was highly associated with total bone volume fraction. To remove any influence of variations in total bone volume fraction, we introduced a new parameter—vertical tissue fraction (vBV/BV). Most interestingly, this new parameter was only weakly associated with total bone volume fraction and yet it retained its high correlation with vertebral strength. Further, both the vertical tissue fraction and total bone volume fraction remained highly significant in a multiple linear regression model to predict vertebral strength. As such, vertical tissue fraction represents a new indicator of bone quality [92, 93]. While requiring confirmation in larger studies, these collective findings demonstrate a new and potentially powerful microarchitectural determinant of vertebral strength.

Our earlier work on isolated specimens of trabecular bone showed a strong association between vertical trabeculae and biomechanical behavior [118, 119]—these new results extend those previous findings to whole vertebrae. In addition to the orientation, the structure of individual trabeculae, *e.g.* plate *vs.* rod, may also have an important effect on biomechanical behavior [87, 118, 122]. Liu *et al.* predicted that more vertical plates fail than vertical rods during axial compression of vertebral trabecular bone [119]. Since the effect of vertical trabeculae reported here includes both plates and rods, it is possible that considering the amount of vertical plates may further improve predictions of vertebral strength. This remains a topic of ongoing research, and may require analyzing images with a higher spatial resolution to accurately characterize the rod-like trabeculae [123]. The excellent agreement between vBV/TV derived from images with a 25 μm voxel size compared to a coarsened 60 μm voxel size ($r^2 = 0.99$ and slope = 0.94 for $n = 19$ samples of tibial trabecular bone; data not shown) suggests that analyzing images with a higher spatial resolution is unlikely to change our conclusions regarding the effect of vBV/TV on vertebral strength.

These findings have potentially important clinical implications for microarchitecture analysis of bone strength. Compared to the role of the traditional microarchitecture parameters (Tb.Th*, Tb.Sp*, Tb.N*, SMI, DA) that we evaluated previously for this same cohort [23] and that has been evaluated by others [25, 121], the vertical tissue fraction parameter, vBV/BV, was more highly associated with vertebral strength and stiffness. In fact, vBV/BV was as good a predictor of vertebral strength as the finite element models ($r^2 = 0.76$, K_{intact} *vs.* F_{ult})—although this may be specific to the compressive loading conditions. Thus, this new parameter may represent an aspect of microarchitecture with the most significance from a biomechanical perspective. Of those same microarchitecture parameters assessed previously [23], only SMI was associated with vBV/BV ($r^2 = 0.64$; $p < 0.001$). Previous studies have shown that trabecular microarchitecture assessed in the spine [46, 124] and at peripheral sites [47, 125, 126] is associated with osteoporotic fracture in the spine. It remains to be seen if this new microarchitecture parameter, whether measured in the spine or at peripheral sites, can improve fracture risk assessment.

Another issue related to the importance of trabecular microarchitecture is the relative role of vertical *vs.* horizontal trabeculae. It is thought that horizontal trabeculae act as stabilizing cross braces to the vertical trabeculae that undergo bending and buckling [40, 41, 119]. However, across individuals, we found that variations in the relative amount of horizontal trabeculae were not associated with variations in vertebral compressive strength. Thus, despite their theoretical importance, variations in the amount of horizontal trabeculae across individuals appear to be much less important than variations in the amount of vertical trabeculae in terms of accounting for observed variations in vertebral strength. We did not address intra-vertebral variations in thickness or spacing of either the vertical or the horizontal trabeculae [117, 127-129]. It is unclear whether considering such variations can further improve assessment of vertebral strength.

A notable feature of this study design was our combined experimental and computational approach, which allowed us to explain the mechanisms associated with the high statistical correlation observed between the amount of vertical trabeculae and vertebral strength. The repeated-measures analysis of the finite element models with *vs.* without the thin cortical shell provided a statistically powerful and unique means of understanding the contribution of the shell to this aspect of whole-vertebral biomechanical behavior. Regarding external validity, the consistency of our findings across a cohort with a wide range of biomechanical properties and morphologies suggests that our findings should apply quite generally, although confirmation in larger and younger cohorts is required. For example, we found that there was only a small effect of variations in the cortical shell, which may have been due to the small variation in cortical mass fraction observed across individuals (mean ± SD = 14.6% ± 3.7%). It is possible that a larger cohort with younger individuals may have greater variations in the cortical shell, which may increase its role.

We focused on compressive loading since functional loads in the spine are primarily compressive in nature [130]. For compression, the stresses in the vertebra are vertically oriented. Since many osteoporotic vertebral fractures are wedge fractures [34], the response to forward flexion may have additional clinical relevance. Forward flexion is not well understood in terms

of how the extra bending moment is distributed between the spinal musculature and the vertebral body [130]. If some of the bending moment is taken up directly by the vertebral body, we would still expect the major load paths to remain vertically oriented since the bending moment would not introduce any multi-axial loads but would instead produce a non-uniform distribution of vertically-oriented stress. This non-uniform distribution would likely result in higher stresses anteriorly [131, 132]. In that case, it is possible that measures of vertical tissue fraction in an anterior region of interest may have additional clinical relevance. However, since predictions of vertebral strength in compression and in bending are correlated [78, 81, 109, 133], any benefits of limiting measures of vertical tissue fraction to an anterior region of interest are not obvious.

One technical issue related to the loading was the manner in which we implemented the uniform compression. We compressed the vertebrae via thin layers of PMMA applied over each endplate. This ignores any possible influence of the intervertebral disc. While the disc condition has a significant influence on vertebral strength [25, 55], it is unclear whether this influence alters the association between the amount of vertical trabeculae and vertebral strength. Hulme *et al.* reported a similar correlation as reported here between total bone volume fraction and vertebral strength for spine segments of similar age that were compressed biomechanically via a disc [25]. This suggests that the presence of the disc may not appreciably alter the association between bone volume fraction and vertebral strength. Moreover, our finding that the major load paths were parallel columns of vertically-oriented bone is consistent with previous work [48, 73, 118, 134] and reflects the overall vertical nature of the loading rather than an artifact of loading via PMMA endcaps. Our previous work suggests that the PMMA endcaps "protect" the vertebral endplates from experiencing high strain [72]. While compressing the vertebra via a disc is expected to place greater loads on the central region of the endplates and on the underlying trabecular bone, the anisotropic structure of the trabecular bone in combination with the vertical nature of the loading suggests that the vertical trabeculae would remain the most structurally important trabeculae and therefore still explain best the variations in vertebral strength. Clearly, additional studies are required to resolve this issue.

In summary, our findings show that variation in vertebral strength across individuals was primarily due to variations in the bone volume fraction of vertical trabeculae. This is because the major load paths in the vertebrae were parallel columns of vertically-oriented bone. The vertical tissue fraction—a new indicator of bone quality—is a potentially powerful microarchitectural determinant of vertebral strength.

Table 3-1: Orientation-related morphology parameters for n = 16 human T9 vertebral bodies.

	Mean	**SD**	**CV (%)**	**Range**
Trabecular bone volume fraction				
Total, BV/TV (%)	13.5	3.3	24.4	7.8 – 18.7
Vertical, vBV/TV (%)	7.2	2.2	30.6	3.9 – 11.4
Oblique, oBV/TV (%)	3.1	0.7	22.6	1.9 – 4.5
Horizontal, hBV/TV (%)	3.2	0.8	25.0	1.9 – 4.5
Trabecular tissue fraction				
Vertical, vBV/BV (%)	52.7	5.2	9.9	45.0 – 64.3
Oblique, oBV/BV (%)	22.2	2.3	10.4	14.5 – 28.3
Horizontal, hBV/BV (%)	24.1	3.8	15.8	19.2 – 26.5

Table 3-2: Independent effect (Pearson's correlation coefficient, *r*) of the orientation-related morphology parameters on measured vertebral strength (F_{ult}), intact vertebral stiffness (K_{intact}), and trabecular stiffness (K_{trab}) for $n = 16$ vertebral bodies.

	F_{ult}	K_{intact}	K_{trab}
Trabecular bone volume fraction			
Total, BV/TV	0.77[c]	0.93[c]	0.90[c]
Vertical, vBV/TV	0.91[c]	0.97[c]	0.95[c]
Oblique, oBV/TV	NS	0.72[b]	0.68[b]
Horizontal, hBV/TV	NS	0.53[a]	NS
Trabecular bone tissue fraction			
Vertical, vBV/BV	0.90[c]	0.71[b]	0.75[c]
Oblique, oBV/BV	-0.55[a]	NS	NS
Horizontal, hBV/BV	-0.76[c]	-0.58[a]	-0.62[b]

[a] $p < 0.05$
[b] $p < 0.01$
[c] $p < 0.001$
NS, not significant

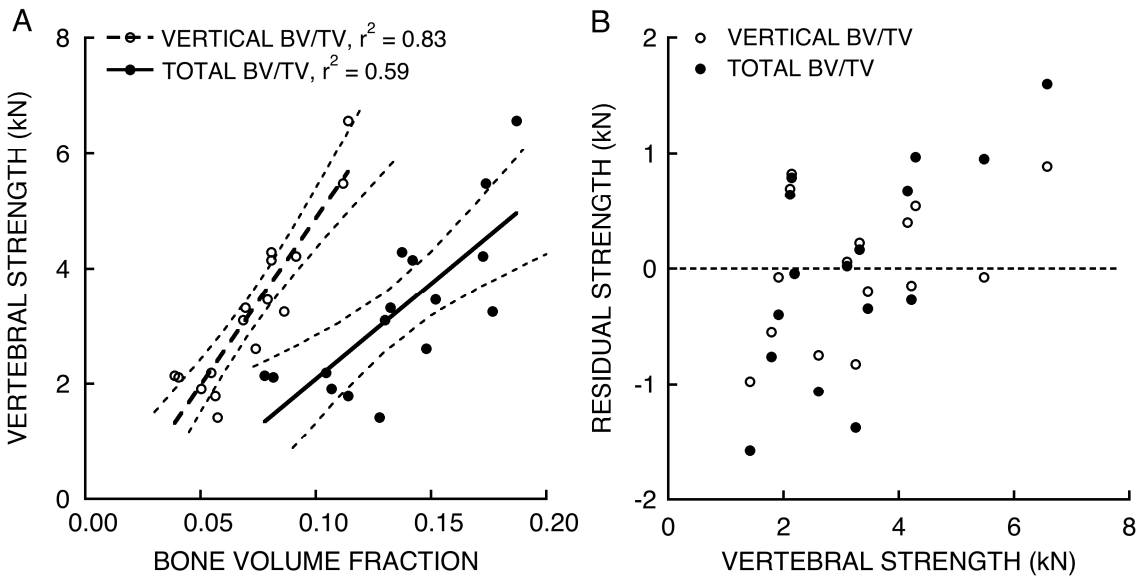

Figure 3-1: Variations in measured vertebral strength were predicted better by variations in the bone volume fraction (BV/TV) of vertical trabeculae than by variations in the BV/TV of all trabeculae. (A) Strength-BV/TV regressions for total BV/TV and vertical BV/TV. Dashed lines show the 95% confidence bands for each fitted line. (B) Residuals from predicted strength using the BV/TV of vertical trabeculae as the predictor (absolute residual = 0.5 ± 0.3 kN) were 20% lower, on average ($p < 0.005$, paired *t*-test), than the residuals from predicted strength using the BV/TV of all trabeculae as the predictor (0.7 ± 0.5 kN).

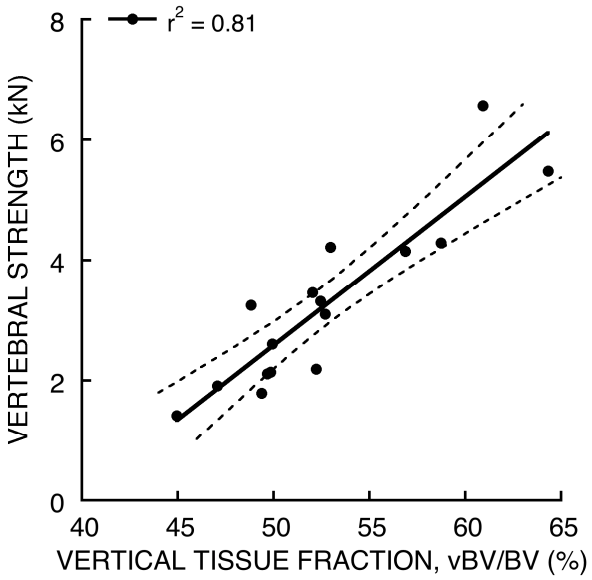

Figure 3-2: Variations in measured vertebral strength were associated with variations in vertical tissue fraction—the bone volume of vertical trabeculae divided by the bone volume of all trabeculae ($p < 0.001$).

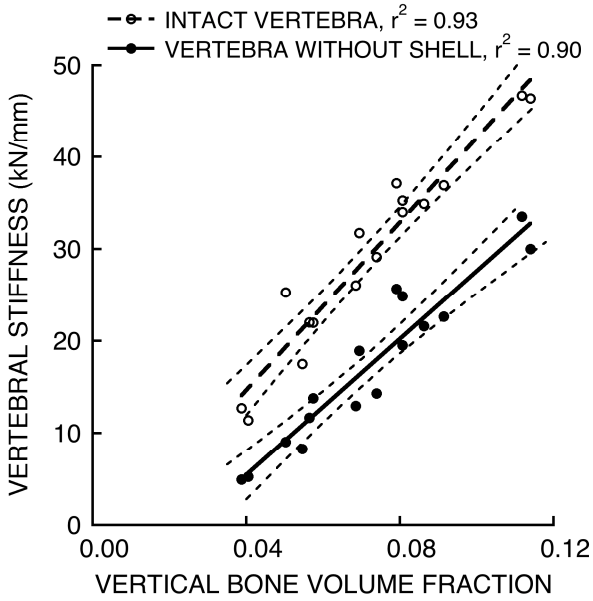

Figure 3-3: Variations in FE-predicted vertebral stiffness for the intact vertebra and for the trabecular compartment were associated with variations in the bone volume fraction of vertical trabeculae.

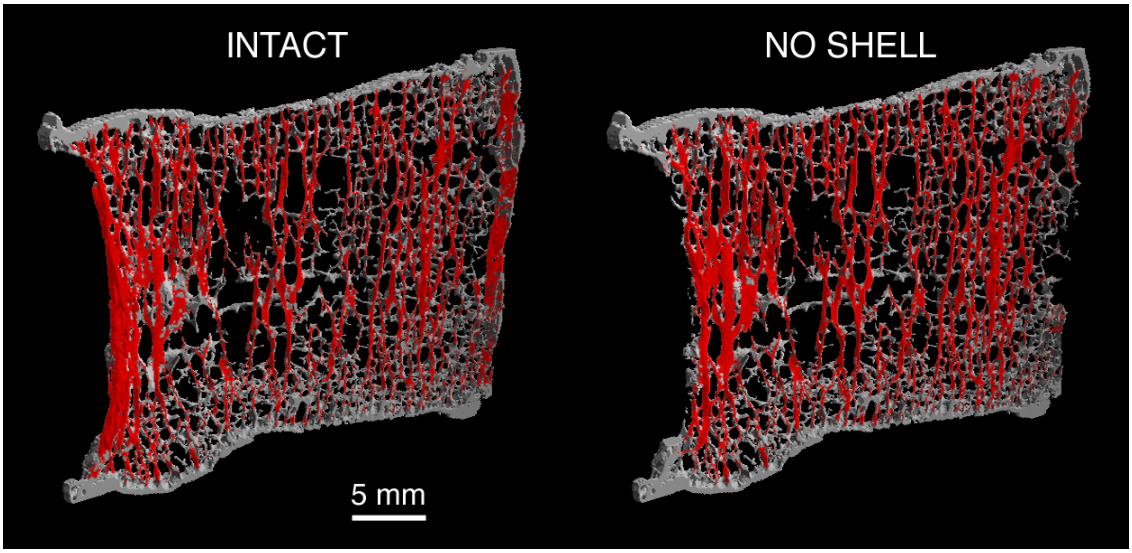

Figure 3-4: Mid-sagittal section, left, from a human T9 vertebra showing the typical load paths—the bone tissue with von Mises stress in the highest quartile, red—predicted by finite element analysis. In this vertebra, ~48% of the load paths belonged to the vertical trabecular bone. Removing the cortical shell, right, did not alter the vertical nature of the load paths.

4. CONTRIBUTIONS OF BONE VOLUME FRACTION AND ARCHITECTURE TO THE FAILURE MECHANISMS IN THE HUMAN VERTEBRA

4.1 Introduction

Understanding the failure mechanisms in the human vertebra—and how they depend on the cortical shell and trabecular microarchitecture—is fundamental to understanding the etiology of the almost 700,00 age-related vertebral fractures that occur each year in the U.S. [1] and as many as 1.4 million that occur each year worldwide [135]. Despite the high incidence of vertebral fractures, the failure mechanisms in the vertebra remain elusive. Part of the reason for this has been the long-standing technical challenge of measuring stress and strain within the vertebra and quantifying the cortical morphology and trabecular microarchitecture so that these measures can be correlated with the failure mechanisms of the same vertebrae. In past biomechanical studies, it was only possible to evaluate strain distributions in thin sagittal sections using texture correlation [54] or to use continuum-type finite element models for stress analysis of the whole vertebra [60, 77-80]. These types of continuum finite element models do not have adequate spatial resolution to capture the thin cortical shell or any aspects of the trabecular microarchitecture; thus, they are not best suited for studying failure mechanisms. One way to overcome these technical limitations is to use higher resolution analysis techniques that can accurately capture the microstructural features of the vertebra and thereby provide detailed insight into the failure mechanisms.

Recent improvements in micro-CT imaging enable the development of high-resolution finite element models that explicitly capture the thin cortical shell and spatially varying trabecular architecture [49, 72, 73], and advances in supercomputing capacity provide the means to analyze multiple vertebrae and thereby account for the biological heterogeneity seen across individuals. However, geometrically nonlinear finite element analysis must be performed to in order to describe certain failure mechanisms in trabecular bone—such as large deformation bending and buckling of trabeculae—which can have an appreciable effect at the apparent yield point [43, 90]. Moreover, this effect is larger in low-density, vertebral trabecular bone [43], which fails due to excessive bending [42, 44, 45, 91] and buckling [136] of rod-like trabeculae. The importance of these failure mechanisms in the whole vertebra—including any potential dependence on bone volume fraction and architecture [40, 41]—remains unclear because vertebral strength and load sharing include a substantial contribution from the cortical shell [48, 51, 113].

Addressing this issue, we employed the latest advances in micro-CT scanning and supercomputing technology to elucidate the failure mechanisms of the human vertebra. Specifically, our objective was to quantify the independent contribution of bone volume fraction (BV/TV) and architecture to the failure mechanisms of the vertebra.

4.2 Methods

Twelve whole T9 vertebrae were obtained fresh-frozen from human cadaver spines (age = 76.9 ± 10.8, 53-97 years; n = 9 male, n = 3 female; BV/TV = 0.14 ± 0.03). None of the donors had a history of metabolic bone disease and all vertebrae showed no radiographic evidence of damage or bone pathologies. The posterior elements were removed and each isolated vertebral body was micro-CT scanned with a 30 μm voxel size (Scanco 80; Scanco Medical AG; Brüttisellen, Switzerland). The scans were coarsened to 60 μm voxel size and the hard tissue and marrow were segmented using a global threshold value. The bone tissue belonging to the trabecular compartment, cortical shell, and endplates was identified and digitally tagged using a custom algorithm (IDL 6.2; ITT Visualization Information Solutions, Boulder, CO USA) [72]. Standard microarchitecture measures—trabecular thickness (Tb.Th), trabecular separation (Tb.Sp), trabecular number (Tb.N), structural model index (SMI), and degree of anisotropy (DA)—were calculated (CTan software; SkyScan, Kontich, Belgium) using the 60 μm images. The average thickness of the cortical shell (Ct.Th) was determined in the transverse region excluding the endplates [49, 72, 73].

High-resolution finite element models of each whole vertebral body were created from the coarsened micro-CT scans by directly converting each 60 μm cubic voxel into an eight-node brick element [23, 72]. A numerical convergence study indicated that this element size accurately captured the inter-specimen variations in yield strength and in the amount of yielded tissue (Appendix 7.1). Materially and geometrically nonlinear finite element analysis was conducted for each model to 1% apparent compressive strain via simulated layers of polymethylmethacrylate (PMMA; elastic modulus 2.5 GPa and Poisson's ratio of 0.3 [105]) placed on the inferior and superior endplates, mimicking boundary conditions commonly used in laboratory compression testing of cadaver vertebrae [80, 101, 102]. All bone tissue was modeled using a rate-independent elasto-plasticity model [43, 137, 138] and homogeneous tissue material properties: elastic modulus 10 GPa [68], Poisson's ratio of 0.3, and tissue-level yield strains of 0.33% and 0.81% (tension and compression, respectively) [43]. Models contained 25-80 million elements and were solved using a highly-scalable [88], implicit parallel finite element framework (*Olympus*). The nonlinear solution algorithm was an inexact Newton method wherein each Newton iteration was solved using a parallel algebraic multigrid solver. All analyses were performed on a Sun Constellation cluster supercomputer (Ranger; Texas Advanced Computing Center, Austin, TX USA) and required up to 2048 processors in parallel and 4 TB of memory. CPU time was 6,000-18,000 hours per analysis (137,000 hours total for all analyses). Visualization of the resulting datasets was performed using a parallel visualization tool (VisIt; Lawrence Livermore National Laboratory, Livermore, CA USA).

Tissue strain distributions were evaluated at the apparent yield point for each vertebra to characterize the failure mechanisms. The apparent yield point was determined from the apparent force-strain curve of each vertebra using the 0.2% offset method, the apparent stiffness being obtained from the first step of the analysis. A validation study indicated that variations in the apparent yield point were highly associated (r^2 = 0.85, p < 0.0001) with variations in measured vertebral strength for the same vertebrae, suggesting the overall validity of the models was good (Appendix 7.2). Our main outcome parameter was the amount of yielded tissue: the percentage of the total number of gauss points in the vertebra that had reached either the compressive or

tensile tissue-level yield strain. The calculation was also performed separately for each compartment—either cortical shell or trabecular bone—and tissue-level yielding mode (tension or compression). Linear regression was used to assess the relationships between the amount of tissue yielded and trabecular bone volume fraction and architecture.

4.3 Results

The amount of yielded tissue was lower in the low-bone volume fraction (BV/TV) vertebrae than in the high-BV/TV vertebrae. At the apparent yield point of the vertebra, the total percentage of tissue exceeding either the compressive or tensile tissue yield strain varied fivefold across vertebrae and increased linearly with BV/TV from just over 3% to more than 17% ($p < 0.005$, Figure 4-1). The percentage of tissue yielding in compression versus tension also increased linearly with BV/TV, the slope for compressive failure being over four times larger than for tensile failure. The ratio of the amount of tissue that had yielded in compression to the amount that had yielded in tension increased linearly with BV/TV ($p < 0.005$, Figure 4-1) such that at low bone volume fractions, the tissue yielding in compression and tension was nearly equal (1:1 ratio) and was localized to opposite sides of slender, rod-like trabeculae that underwent excessive bending (Figure 4-2). For stronger, high-bone volume fraction vertebrae, the tissue yielding in compression was up to four fold greater than in tension, and was widespread throughout the vertical, load-bearing trabeculae and the cortical shell.

Substantially more of the yielded tissue belonged to the trabecular bone than to the cortical shell, and the relative amounts of tissue that yielded in each compartment depended on BV/TV. Of the tissue that had yielded in compression at the apparent yield point of the vertebra, the percentage belonging to the trabecular bone (64.2 ± 4.2%) was over three-fold greater, on average, than the percentage of tissue belonging to the cortical shell (20.4 ± 4.2%; $p < 0.0001$ paired *t*-test). Similarly, the overwhelming majority of the tissue that had yielded in tension also belonged to the trabecular bone (73.3 ± 6.7% *vs.* 8.6 ± 2.3% in the cortical shell; $p < 0.0001$ paired *t*-test). On a relative basis, between ~10-35% of the trabecular bone and ~5-35% of the cortical shell yielded, and in both compartments, the total amount of yielded tissue increased with BV/TV (Figure 4-3). In the low-BV/TV vertebrae, the amounts yielded tissue in tension and in compression were nearly equal in both compartments. In the high-BV/TV vertebrae, the ratio of yielded tissue in compression-to-tension was almost four times greater for the cortical shell than for the trabecular bone (Figure 4-4).

Of all the microarchitecture parameters, only trabecular number ($r = 0.60$, $p < 0.05$) and structural model index ($r = -0.54$, $p = 0.07$) were correlated with the total amount of yielded trabecular tissue. The ratio of the amount of trabecular tissue that had yielded in compression to the amount that had yielded in tension was not significantly correlated with any of the microarchitecture parameters ($p = 0.14$-0.57). The tissue yielding outcomes derived for the cortical shell were not significantly correlated with any of the microarchitecture parameters ($p = 0.10$-0.94).

4.4 Discussion

The results of this study showed that trabecular bone volume fraction (BV/TV) and architecture have an appreciable effect on vertebral strength via their contribution to the failure

mechanisms in the vertebra. Low-BV/TV vertebrae failed due to localized bending of slender, vertical trabeculae, which led to concentrated yielding at the tissue-level. Thus, only a small percentage of the tissue yielded when the bone reached the apparent yield point. In contrast, more tissue yielded in the high-BV/TV vertebrae because widespread material yielding in the cortical shell and vertical trabeculae preceded trabecular bending. Taken together, these findings illustrate a new aspect of vertebral fragility: as bone volume fraction decreases with aging and disease, not only is the vertebra becoming weaker, but it is also becoming much less structurally robust and more susceptible to overloads.

Previous efforts to characterize the failure mechanisms in the human vertebra using high-resolution finite element modeling were limited to linearly elastic behavior; here, fully nonlinear modeling enabled us to characterize the failure mechanisms during an isolated overload. Load sharing between the cortical shell and the trabecular compartment at lower compressive loads involved the vertical trabeculae [48, 139], which supported the highest loads near the endplates [49, 72, 73]. In low-BV/TV vertebrae, there were fewer of these vertical load paths, and our new findings showed that at higher loads, the strain field localized to the slender, vertical trabeculae and to their horizontal supports. The yielding of tissue within these vertical trabeculae and the lack of alternative load paths may help explain why reductions in vertebral strength following an isolated overload tend to be greater in low-density vertebrae [102].

Earlier work on isolated specimens of trabecular bone showed that the total amount of yielded tissue and the relative amounts of compressive *vs*. tensile yielding depended on the bone volume fraction and architecture of the trabecular bone [44, 45]—these new results extend those previous findings to whole vertebrae. The compressive and tensile yielding predicted for the vertical and horizontal trabeculae, respectively [119], is also consistent with the present findings for whole vertebrae. These collective findings suggest that the presence of the cortical shell may not appreciably alter the failure mechanisms in the trabecular bone; indeed, the roles of the cortical shell and the trabecular bone in vertebral failure behavior appear to be largely independent.

This study is the first to use fully nonlinear, high-resolution finite element analysis of whole vertebral bodies to assess vertebral strength. As expected from previous studies using human vertebral trabecular bone [79, 140], variation in predicted yield strength was highly associated with experiment-measured ultimate strength for the whole vertebral bodies. Direct comparisons of yield strength between the models and the experiments were not possible since strain measurements—which are sensitive to machine compliance and possible gaps between the PMMA and endplates—were unavailable from the experiments. Converting the measurements of ultimate strength to yield strength (Ultimate strength = 1.2 * Yield strength [79]) revealed that the models overestimate yield strength by a factor of two. In addition to possible errors related to discretization [141, 142] and coarsening [143, 144], subtle differences in thresholding can also result in substantial errors in finite element-derived mechanical properties for trabecular bone [68]. High-resolution finite element models of trabecular bone accurately predict yield strength when the images are thresholded to match experimental measurements of bone volume fraction [43, 86]. A similar metric for choosing the threshold may improve the accuracy of finite element-derived strength predictions of whole bones. Nevertheless, the high correlation between the

model predictions and experimental measurements as well as the quantitative and qualitative similarities between the trends for tissue yielding reported here and those reported for isolated specimens of trabecular bone that were thresholded to match bone volume fraction [44, 45] suggests that the current modeling approach should capture the relative variations in failure mechanisms.

The main novelty of this study was the application of fully nonlinear, high-resolution finite element modeling to a modestly sized cohort of whole vertebral bodies. These finite element models had material nonlinearities to account for the strength asymmetry of the bone tissue and geometric nonlinearities to simulate the effects of large deformations. Identifying the thin cortical shell allowed us to compare for the first time the relative failure behavior of the cortical and trabecular compartments. In its use of high-resolution micro-CT imaging, high-performance supercomputing, validated material constitutive models, and efficient solver algorithms, this study represents the state-of-the-art in computational modeling of whole-bone failure behavior.

Despite these overall strengths, certain limitations in our modeling approach should be noted. Most important, the finite element analyses ignored any possible influence of variations in tissue mineralization. While inter-individual variations in tissue mineral density are small [110] and intra-individual variations have only a modest influence on apparent-level elastic properties [145, 146], the effect of these variations on the tissue-level strain distributions at apparent-level yield remains unknown. A second limitation of the finite element analyses was the absence of damage or softening behavior in our constitutive model. Recent work suggests that damage and softening may be important for predicting post-yield behavior [147]. However, our focus here was on the failure mechanisms that lead to the onset of apparent yielding, and the lack of observed micro-fracture of trabeculae at the apparent yield point [85, 148, 149] suggests that including such behavior should not be important in our models.

An additional limitation was that the vertebrae were loaded in a manner that is not fully representative of *in vivo* loading. Compressing the vertebrae via PMMA endcaps ignores any possible influence of the intervertebral disc. Although the disc condition has a significant influence on vertebral strength [25, 55], it is unclear whether this influence alters the failure behavior of the cortical shell and the trabecular bone. Previous work suggests that the PMMA endcaps preferentially load the cortical shell and that loading the vertebra via a disc may increase the stresses on the trabecular bone [72]. In that case, loading the vertebra via a disc would decrease the amount of yielded tissue in the cortical shell. However, the loads on the trabecular bone would still be vertically oriented, and thus, the trabecular bone would exhibit similar failure mechanisms—including the dependence on BV/TV—as those reported here. Clearly, additional studies are required to address this issue, and more complex loading such as combined compression and flexion [131, 132] should also be considered.

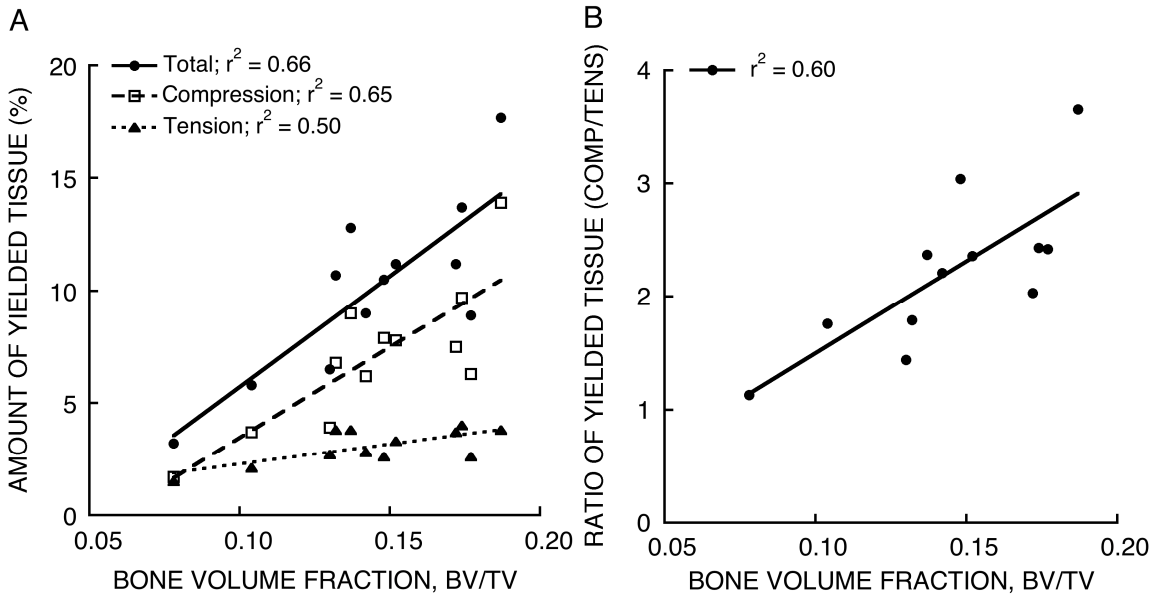

Figure 4-1: Amount of yielded tissue in the vertebra depended on bone volume fraction (BV/TV). (A) The total amount of yielded tissue ($p < 0.005$), as well as the amounts of yielded tissue in compression ($p < 0.005$) and in tension ($p < 0.01$) increased with BV/TV. (B) The ratio of the amount of tissue yielded in compression to the amount of tissue yielded in tension increased linearly with BV/TV ($p < 0.005$).

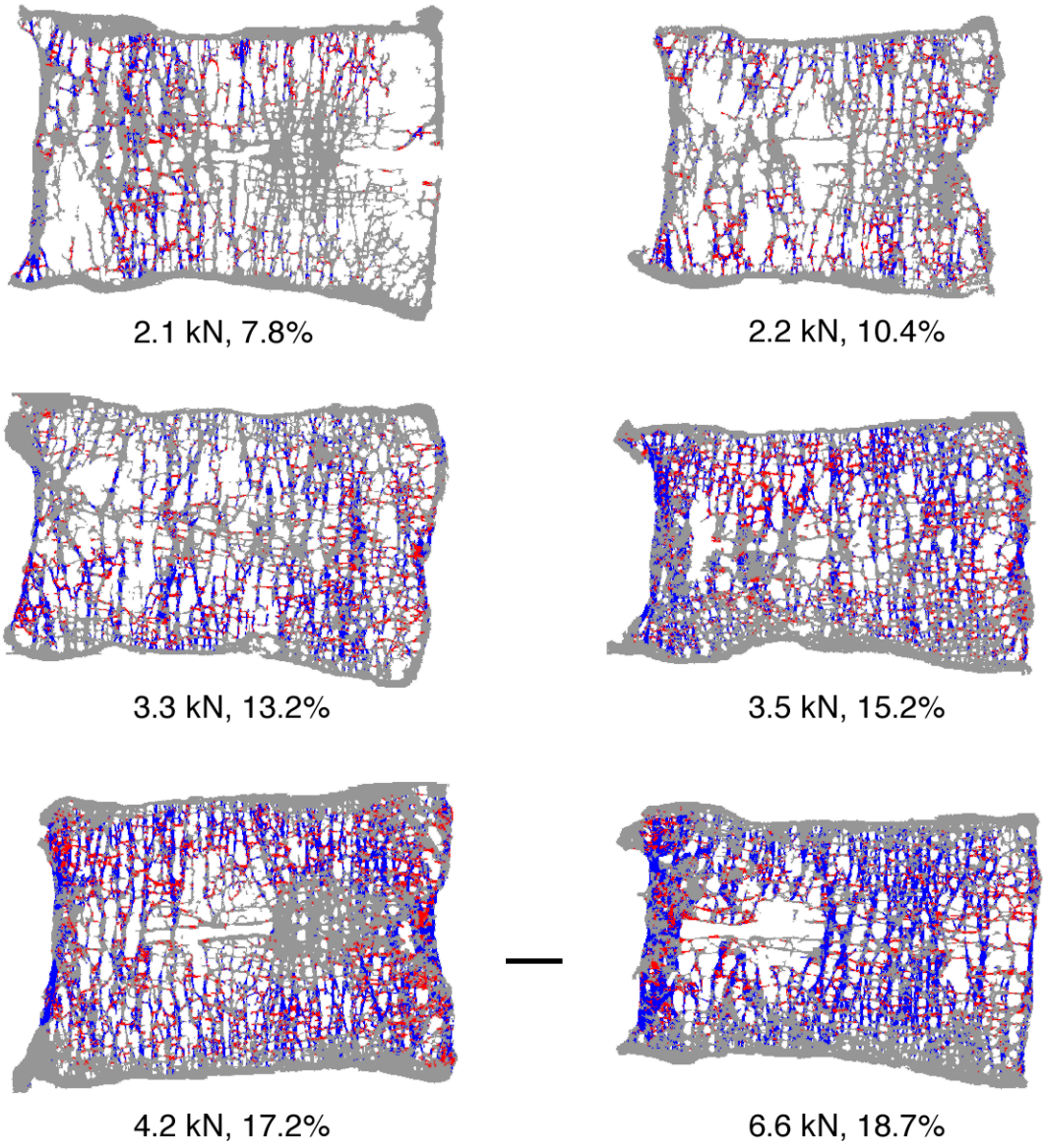

Figure 4-2: Mid-sagittal sections from six human T9 vertebrae showing the distribution of yielded tissue in compression (blue) and in tension (red) at the apparent yield point of each vertebra. Vertebrae are arranged (from left to right and top to bottom) in order of increasing vertebral strength and bone volume fraction. Note that the trabeculae, cortical shell, and endplates appear thicker than they actually are because all of the bone tissue in the 1 mm-thick section is projected onto a single plane. Data given as: vertebral strength, bone volume fraction. Scale bar: 5 mm.

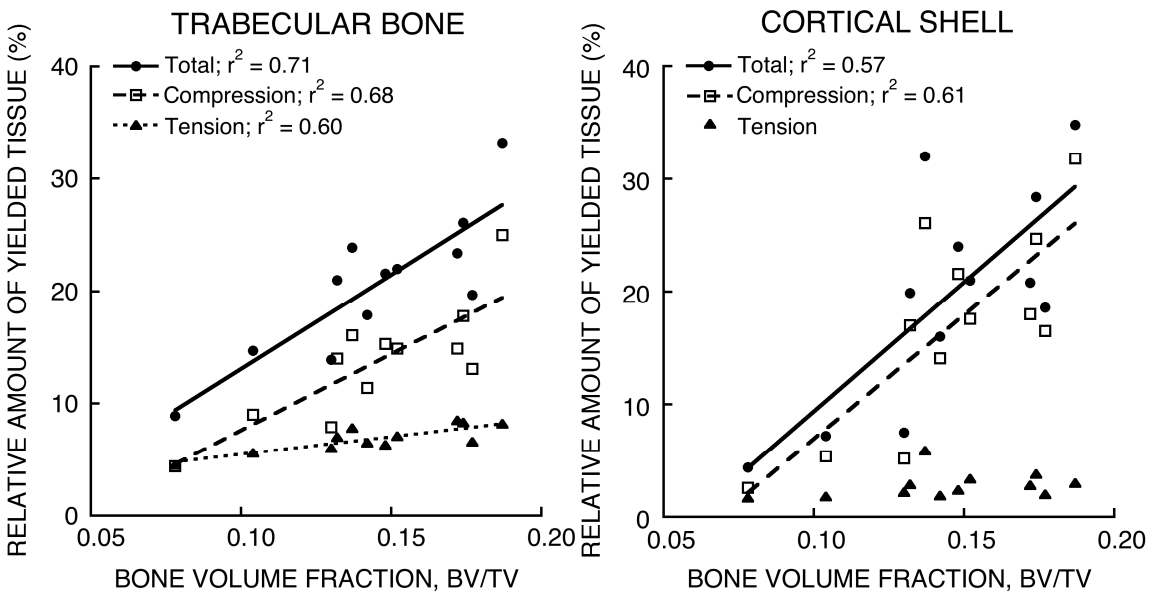

Figure 4-3: The relative amounts of yielded tissue (*i.e.* amount of yielded tissue in each compartment relative to the total amount of tissue in that compartment) for the trabecular bone and in the cortical shell depended on bone volume fraction (BV/TV). In the trabecular compartment, the total amount of yielded tissue ($p < 0.001$), as well as the amounts of yielded tissue in compression ($p < 0.001$) and in tension ($p < 0.005$) increased with BV/TV. In the cortical shell, only the total amount of yielded tissue ($p < 0.005$) and the amount of yielded tissue in compression ($p < 0.005$) increased with BV/TV.

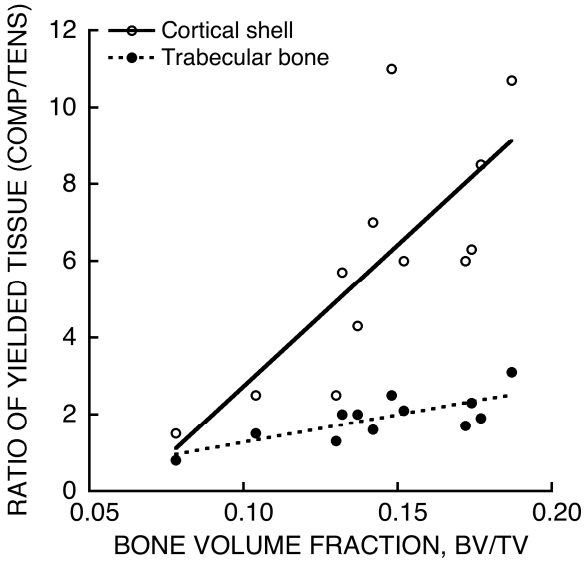

Figure 4-4: The ratio of the amount of tissue yielded in compression to the amount of tissue yielded in tension in the trabecular bone ($r^2 = 0.55$, $p < 0.005$) and in the cortical shell ($r^2 = 0.58$, $p < 0.01$) increased linearly with bone volume fraction (BV/TV).

5. MECHANISMS OF INITIAL ENDPLATE FAILURE IN THE HUMAN VERTEBRA

5.1 Introduction

Osteoporotic vertebral fractures frequently involve the endplates of the vertebral body [61-64, 150, 151]. It has been suggested that the involvement of the endplates may even distinguish a vertebral fracture from a vertebral deformity [36]. Understanding the mechanisms of endplate failure may therefore provide insight into the etiology of osteoporotic vertebral fractures.

The mechanisms underlying endplate failure remain unclear. Despite overall direct compressive loading of the vertebra by the intervertebral disc, there is evidence that appreciable levels of tensile strain can develop at the endplates [152, 153], perhaps due to the fluid-like behavior of the intervertebral disc [57, 72]. The development of large tensile strain is significant biomechanically because bone tissue is weaker in tension than in compression [68, 86, 154] and thus any factors—such as the material behavior of the intervertebral disc—that contribute to the development of high tensile strain in the endplates may have an important role in vertebral fragility. However, the relative magnitude of the tensile strains in the endplates versus that of the cortical shell and trabecular centrum has never been quantified, nor has the relative magnitude of tensile and compressive strains in the vertebra been compared generally. Thus, it is not clear if the development of high tensile strains in the endplate is an important factor that might predispose the vertebral body to early failure and what role, if any, the disc may have on this. Addressing this issue, we sought to determine the location of the highest tensile strains within the vertebral body and the influence of the material behavior of the disc on such strains.

5.2 Methods

Since measuring tissue-level strains in the endplates, cortical shell, and trabecular bone would be very difficult to perform using direct biomechanical testing, we assessed tissue-level strains by performing high-resolution, micro-CT-based finite element analysis on 22 elderly human vertebral bodies in which the vertebral bodies were virtually compressed through simulated intervertebral discs. To determine the regions within the vertebra that are likely to fail in tension and compression, we used the finite element analysis of each vertebra to identify the most highly strained tissues by type—either tension or compression—and compared the amount of highly-strained tissue of each type across the different compartments: endplates, cortical shell, and trabecular bone. Since the tissues having the highest strains with respect to the tensile and compressive yield strains are likely to fail first, we also compared the relative magnitudes of the highest tensile and compressive tissue strains across the different compartments after normalizing these strains to their respective yield strains. The influence of Poisson-type expansion of the disc on these results was determined by virtually compressing the vertebral bodies a second time in which the Poisson expansion was suppressed. The change in the amount of highly-strained tissue within each compartment after suppressing the Poisson expansion was calculated for all of the vertebral bodies.

Twenty-two human T9 whole vertebral bodies were obtained fresh-frozen from cadavers (n = 11 male; n = 11 female; age range: 53-97 years, mean ± SD = 81.5 ± 9.6 years) with no medical history of metabolic bone disorders. As described elsewhere [23], the posterior elements were removed and each isolated vertebral body was micro-CT scanned using a 30 μm voxel size

(Scanco 80; Scanco Medical AG, Brüttisellen, Switzerland). The scans were coarsened to 60 μm voxel size and the hard tissue and marrow were segmented using a global threshold value (Scanco). The bone tissue in the resulting images was then compartmentalized (Figure 5-1) using a custom algorithm (IDL 6.2; ITT Visual Information Solutions, Boulder, CO USA) with moving averages to identify the endplates and the cortical shell [49, 72].

High-resolution finite element models of each vertebral body were created from the coarsened micro-CT scans [23, 72]. Briefly, each 60 μm-sized cubic voxel in the coarsened scans was converted into an 8-noded finite element and tagged with a unique identifier corresponding to its compartment: endplates, cortical shell, and trabecular bone. Since the transition from the endplates to the cortical shell is inexact, the bone tissue at the corner regions of the vertebral body was also tagged [72] and excluded from further analysis. The intervertebral discs adjacent to each vertebral body were simulated by virtually adding discs to the superior and inferior endplates. Thoracic discs have the most uniform height [53] and thus, a disc height of 5 mm was modeled for each vertebra using symmetry boundary conditions at the mid-transverse plane of the disc [49, 72].

Material properties in the finite element models were assigned based on whether the element belonged to the bone tissue within the vertebral body or the soft tissue within the discs. All bone tissue belonging to the vertebral body was given homogeneous elastic and isotropic material properties (elastic modulus of 10 GPa [68] and Poisson's ratio of 0.3) since the cortical shell is often described as condensed trabeculae [17-19] and since the anisotropy of trabecular tissue has only a minor role on trabecular behavior [84]. Furthermore, these assumed material properties were used for all vertebrae since the coefficient of variation in mean tissue mineral density—one determinant of differences in tissue elastic modulus amongst individuals—for human trabecular bone is less than about 2% [110]. For the soft tissue belonging to the intervertebral disc, we assigned homogeneous elastic and isotropic material properties typical of a semi-degenerated disc that still retains its fluid-like properties (elastic modulus of 8 MPa [155] and Poisson's ratio of 0.45 [56, 156, 157]) since the mean age of the cadavers was 82 years and since degenerated discs are more uniform than are healthy discs [58, 59].

Loads on the vertebral bodies were simulated in the finite element models to mimic compressive loading. In all of the models, the top surface of the disc was displaced in the superior-inferior direction. The magnitude of the applied displacement was a constant percentage (1%) of the original height of the model to facilitate comparison of the results across multiple vertebrae exhibiting considerable heterogeneity in size and shape. Roller-type constraints at the mid-transverse plane of each disc were used to model the symmetry boundary conditions.

The resulting finite element models had up to 80 million elements and over 300 million degrees of freedom and required specialized software and hardware for analysis. All computations were performed using custom code—including parallel mesh partitioner and algebraic multigrid solver [88]—on an IBM Power4 supercomputer (Datastar; San Diego Supercomputing Center, San Diego, CA USA). Typical hardware requirements for a single analysis comprised 880 processors and 1800 GB total memory. The average CPU time was 115 hours (11 minutes in real-time).

To determine the effect of the Poisson expansion of the disc on the strains in the bone, a second finite element analysis was performed for each vertebra in which we suppressed such behavior. The Poisson expansion of the disc under compression arises in part from its high water and proteoglycan content, which pressurizes the nucleus [52]. Without Poisson expansion, a disc under axial compression would not expand transversely. We simulated this condition by compressing the vertebrae via discs with a Poisson's ratio of zero. Rather than model the physiological condition of the disc, our goal was to create a large change in the disc's behavior to determine how the strains in the vertebra are sensitive to such a change.

A number of outcomes from the finite element analyses were used to identify the most highly strained bone tissue in the models. The 90^{th} percentile limits of the maximum and minimum principal strains were first calculated for each vertebral body [72]. Any bone element having either its maximum principal strain or minimum principal strain beyond the corresponding strain limit for that vertebra was classified as "highly-strained". The proportion of highly-strained tissue in tension and in compression within each compartment (*i.e.* endplates, cortical shell, and trabecular bone) was expressed as a percentage of the total amount of highly-strained tissue in that compartment. To compare the magnitudes of the highest tensile and compressive strains across the various compartments, the 90^{th} percentile limits of the maximum and minimum principal strains were calculated separately for the endplates, cortical shell, and trabecular bone. A higher strain limit for one compartment is one indicator that the highest tissue strains within that compartment are greater than the highest tissue strains within a compartment having a lower strain limit. To identify the tissues with the greatest risk of initial failure, the strain limits for each compartment were normalized by estimates of the effective yield strains for vertebral bone tissue (tension = 0.34%; compression = -0.69% [68]).

The proportion of highly-strained tissue in tension and in compression was compared across compartments using paired *t*-tests with Bonferroni adjustments for multiple comparisons. Similarly, paired *t*-tests with Bonferroni adjustments were also used to compare across compartments the mean values of the maximum and minimum principal strain limits and the risks of initial failure. The change in the amount of highly-strained tissue in tension and in compression in each compartment due to suppression of Poisson expansion of the disc was determined twofold: 1) a single-group *t*-test with Bonferroni adjustment to determine if the change was statistically different from zero, and 2) a paired *t*-test with Bonferroni adjustments to determine if the change was statistically different across compartments. All tests were taken as significant at $p < 0.05$.

5.3 Results

During the simulated compressive loading of the vertebral body, the endplates were more highly strained in tension than were the trabecular bone and the cortical shell, whereas the latter two were more highly strained in compression (Figure 5-2). Across all 22 vertebrae, an average (mean ± S.D.) of 96.6 ± 1.2% of the highly-strained tissue within the endplate was strained in tension (Figure 5-3), which was more than twice the proportion of highly-strained tissue in tension in the trabecular bone (45.6 ± 4.0%) and cortical shell (30.7 ± 11.8%). With respect to anatomical location, the highly strained tissue in the endplates comprised a larger amount of the

tissue belonging to the superior endplate (27.7 ± 7.7%) than to the inferior endplate (20.8 ± 6.6%; $p < 0.002$ paired *t*-test).

The bone tissue within the endplates, which had higher absolute values of tensile strains than either the bone tissue within the trabecular bone or the cortical shell, also had the greatest risk of initial failure (Table 5-1). The 90th percentile compressive strain limit was higher for the bone tissue within the trabecular compartment than for the bone tissue within the other two compartments, but when the magnitude of the tensile and compressive strain limits was normalized by the assumed magnitude of the yield strains in tension and in compression, respectively, the tissue belonging to the endplates that was highly strained in tension had the greatest risk of initial failure (Table 5-1). Initial failure of tissue in compression was not likely in the endplates but was most likely in the trabecular bone. These trends were similar when different assumed values of the yield strains were used (tension = 0.40%; compression = -0.62% [68]).

The development of these high tensile strains in the endplates was directly associated with the Poisson-type expansion of the intervertebral disc (Figure 5-4). When Poisson expansion was virtually suppressed, the amount of highly-strained endplate tissue in tension decreased by 79.4 ± 11.3% (Figure 5-5). Removing this behavior increased the amount of highly-strained tissue in tension belonging to the trabecular bone and cortical shell, with the effect being two-fold greater for the latter. For the endplates, suppressing the suppressing Poisson expansion of the disc reduced the total amount of highly-strained tissue more in the superior endplate (-80.6 ± 12.3%) than in the inferior endplate (-73.1 ± 15.0%; p=0.005 paired *t*-test).

5.4 Discussion

These findings support the concept that endplate failure may be an etiologic factor in osteoporotic vertebral fracture. Specifically, our findings indicate that initial failure of the vertebra is associated with the development of high tensile strains within the endplate, which in turn is influenced by the material behavior of the disc. Our previous work has shown that the general behavior of the endplates during compressive loading of the spine is sensitive to the material properties of the intervertebral disc [72]. In cadaver experiments which observed frequent endplate failures, variations in proteoglycan content of the disc were associated (r^2 = 0.70) with variations in vertebral compressive strength [25], but the link between the variations in disc properties and the mechanism of endplate or vertebral failure was unclear. Our new data provide a mechanistic link between endplate failure, initial vertebral failure, and the material behavior of the disc.

One notable element of this study was our use of high-resolution micro-CT-based finite element modeling to estimate the tissue-level strains within the human vertebral body. This approach enabled us to probe the mechanisms of initial failure of the endplate using a repeated measures-type study design in which changes in tissue-level strains were directly attributable to virtual suppression of the fluid-like properties of the disc. Furthermore, we applied this technique to a moderately sized cohort of human vertebrae, thus accounting for typical variations in vertebral morphology in the elderly and providing a reasonable degree of external validity to our results. For example, the remarkable consistency in the proportion of highly-strained endplate

tissue in tension across all 22 vertebrae analyzed—97% on average with a standard deviation of only 1.2%—suggests that this trend is likely to persist in the general population of elderly vertebrae.

One limitation of this study is that by performing linear analyses, we could address only regions of initial failure, which may not represent the locations of final failure at the point of structural collapse of the vertebra. Comparison of the regions of initial failure from a linear analysis with regions of failure computed using fully non-linear modeling [72] did confirm the validity of the former. However, localized large-deformation effects [43, 90, 158] may cause the tissue in slender trabeculae to fail before the tissue in thicker trabeculae fails [90, 136], and hence, the total amount and distribution of tissue failure that occurs when a vertebra's strength is exceeded may depend on the morphology of the bone [45, 159]. Thus, further work using non-linear modeling carried out to relatively large apparent strains (>10%) is required in order to extend these findings to the structural collapse of the vertebra.

An additional limitation is that we assumed a homogeneous elastic and isotropic model for the intervertebral disc. The material behavior of the disc is complex, including material non-linearity, time dependence, and intra- and inter-specimen heterogeneity [160-162]. Previous finite element analyses of bone-disc complexes have accounted for some of this complexity, but have omitted inter-specimen heterogeneity and have treated the vertebra in a relatively simplistic fashion [56, 57, 155, 163]. Here, we chose instead to model the bone in detail, since we were interested in understanding how the tissue-level strains in the vertebra were influenced by some of the dominant material characteristics of the disc. Our finding that the central endplates are highly strained in tension and that these tensile strains are associated with the material behavior of the disc is consistent with results from more sophisticated models of the disc [56, 57]. Moreover, our finding that the superior endplate was more vulnerable than the inferior endplate is in agreement with Bay *et al.* and Zhao *et al.* who accounted for the effects of intra- and interdiscal variations in disc behavior via direct biomechanical testing. Together, these similarities suggest that our simple disc model was sufficient for exploring general trends regarding the role of disc behavior on the mechanisms of vertebral failure. Further work is required to integrate sophisticated modeling of both the bone and the disc. Our results indicate that such analyses may provide new insight into the interaction between the bone and the disc as it pertains to vertebral strength.

The results of this study are consistent with and complementary to previous work that associated disc health with endplate failure in the etiology of vertebral fractures [25, 55, 72, 164] and taken together, this body of work suggests disc material properties may influence vertebral strength via their effect on the development of high tensile strains in the endplates. Endplate strength is negatively influenced by the proteoglycan content within the nucleus of the disc [25]. The high concentration of proteoglycans in the nucleus of healthy discs pressurizes the central region of the disc [52, 53]. During axial loading, the pressurized nucleus directs the load to the center of the endplates [54-57]—the thinnest [20] and weakest [165] region. Complementary, our results showed that the central region of the endplates is highly strained in tension, a loading mode in which bone is biomechanically weak. As the disc degenerates, in contrast, our results predict a shift in load from the endplates to the cortical shell. This shift in load agrees with

previous findings [56, 57, 60] and may contribute to stress shielding of the anterior vertebra [131, 132] and explain the observed increases in vertebral strength with disc degeneration [25].

Our finding that the endplates were highly strained in tension is notable because bone tissue is weaker in tension than in compression, and because the type of tensile strains in the endplates may be more harmful than those in the other compartments. Uniaxial tension occurs in the axial trabeculae and cortices that bend under the applied compressive loads and in the transversely trabeculae that resist such bending. In contrast, a detailed analysis of the endplates revealed that *biaxial* tension exists in the plane of the endplate due to the Poisson expansion of the disc (Appendix 7.3). Little is known about the failure behavior of bone tissue in biaxial tension; one hypothesis is that biaxial tension is particularly harmful because existing microdamage may be less able to "escape" the crack-propagating effects of this type of loading compared to uniaxial tension. Further work is recommended to understand the failure behavior of the endplates in biaxial tension and its dependence on the behavior of the intervertebral disc.

In summary, our findings reveal two striking characteristics of the endplates that help to explain their frequent involvement in osteoporotic vertebral fractures: the endplates are at the highest risk of initial failure due to the development of high tensile strains, and the development of such high tensile strains is directly associated with the material behavior of the intervertebral disc.

Table 5-1: Maximum and minimum principal strain limits (90^{th} percentiles) for bone tissue in the endplate, trabecular bone, and cortical shell.

	Endplate	Trabecular Bone	Cortical Shell
Maximum Principal Strain			
90^{th} Percentile (μstrain)	836 ± 237 [a,b]	600 ± 139 [b]	437 ± 111
Risk of Initial Failure[c]	0.25 ± 0.07	0.18 ± 0.04	0.13 ± 0.03
Minimum Principal Strain			
90^{th} Percentile (μstrain)	-525 ± 126 [a,b]	-1085 ± 232 [b]	-861 ± 162
Risk of Initial Failure[c]	0.08 ± 0.02	0.16 ± 0.03	0.12 ± 0.02

Data given as mean ± SD (n = 22 vertebral bodies)
[a] $p < 0.0001$ *vs.* trabecular bone
[b] $p < 0.0001$ *vs.* cortical shell
[c] The maximum and minimum principal strain limits (90^{th} percentiles) were normalized by the respective yield strains (tension = 0.34%; compression = -0.69% [68]) to determine the relative risk of initial failure. Compared to a lower number, a higher number indicates a greater relative risk of initial failure. Pairwise comparisons between each of the risks of initial failure were significantly different ($p < 0.0001$) except for the comparison between the risk of initial failure in the cortical shell in tension and in compression.

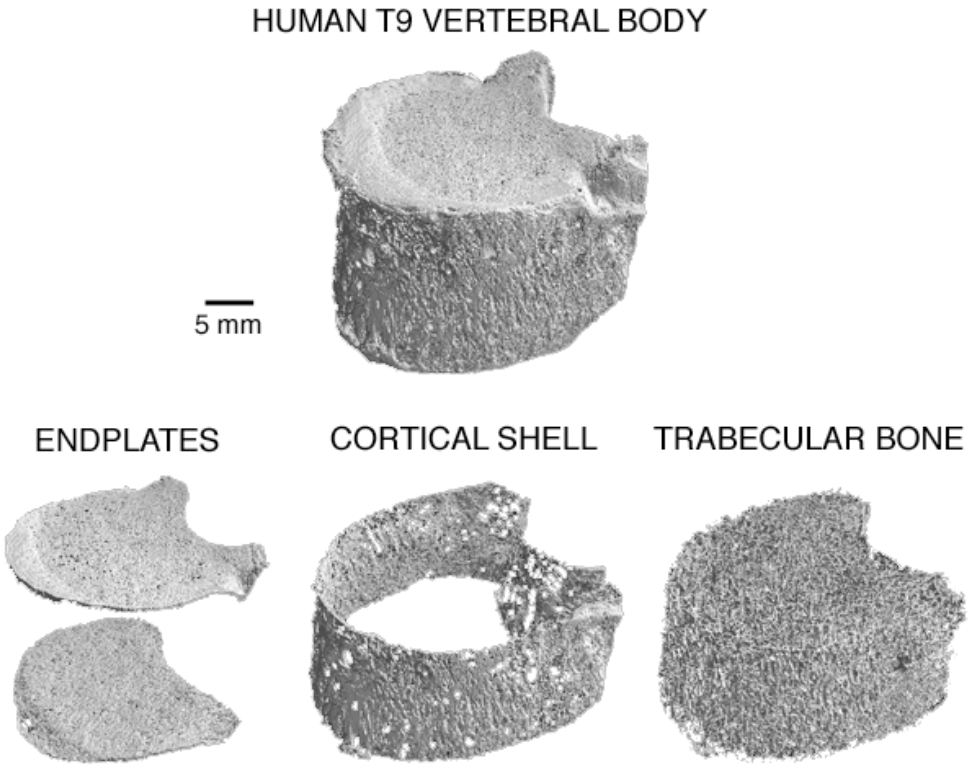

Figure 5-1: Micro-CT rendering of a human T9 vertebral body (top) compartmentalized into the endplates (bottom, left), cortical shell (bottom, center), and trabecular bone (bottom, right). Donor information: 82 year-old male.

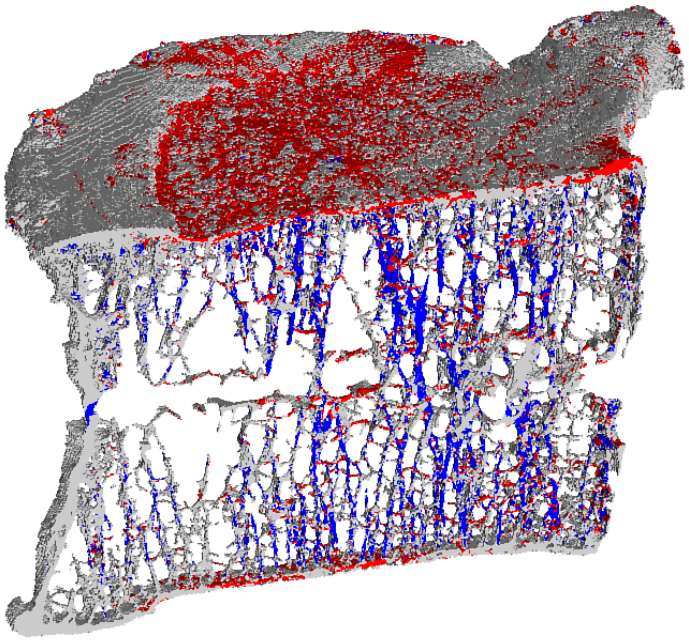

Figure 5-2: Mid-sagittal cutaway from a human vertebral body showing the typical distribution of highly strained tissue in tension (red) and in compression (blue) predicted by finite element analysis. The bone tissue behind the para-sagittal slice (1 mm thick) and below the superior endplate has been removed from the image for clarity.

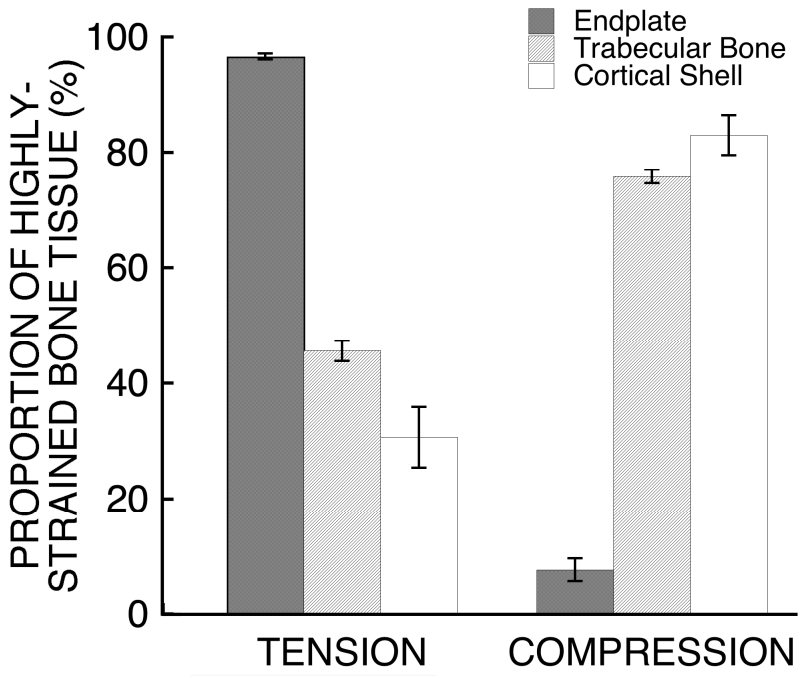

Figure 5-3: Comparison of the relative proportion of bone tissue highly strained in tension and in compression between the endplates, trabecular bone, and cortical shell. All comparisons were significantly different ($p < 0.0001$). Error bars show 95% CI ($n = 22$ vertebral bodies).

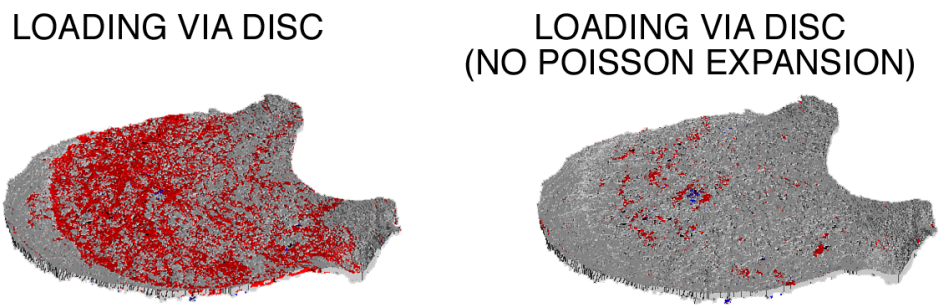

Figure 5-4: Distribution of highly strained tissue in tension (red) and in compression (blue) within the superior endplate of a human vertebral body when loaded via simulated intervertebral disc (left). Removing the Poisson expansion of the disc led to a 96% reduction in the total amount of highly-strained endplate tissue (inferior + superior) for this vertebral body (right).

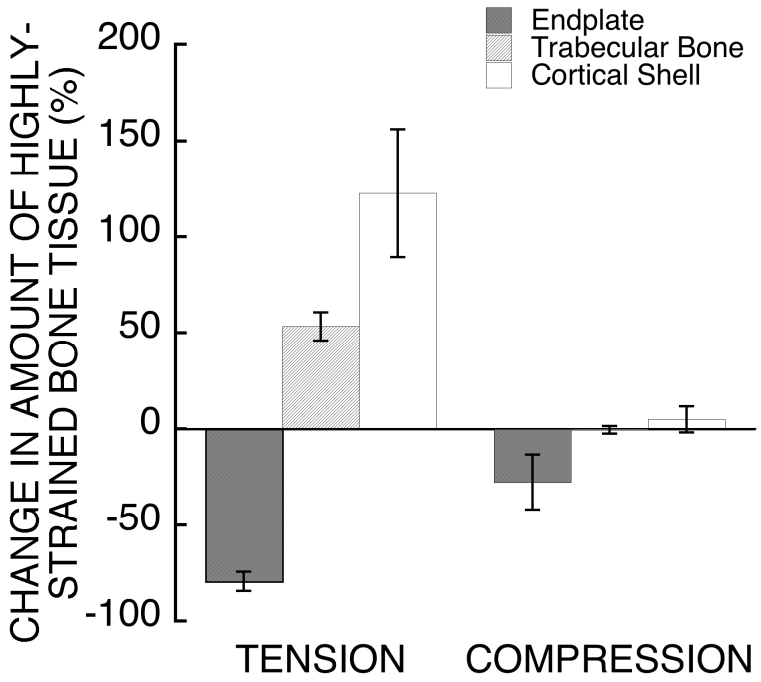

Figure 5-5: Comparison of the effect of suppressing the Poisson expansion of the disc on the amount of highly-strained tissue in tension and in compression between the endplates, trabecular bone, and cortical shell. The change in the amount of highly-strained tissue in tension was significantly different between the three groups ($p < 0.0001$). The change in the amount of highly-strained tissue in compression was significantly different for the endplates only ($p < 0.0001$ endplates *vs.* cortical shell and endplates *vs.* trabecular bone). Error bars show 95% CI ($n = 22$ vertebral bodies).

6. CONCLUSIONS

The overall goal of this research was to enhance the current understanding of the biomechanical mechanisms of vertebral strength and the etiology of vertebral fractures. The findings of this research are both scientifically and clinically significant. From a basic science perspective, substantial insight was gained into the failure mechanisms of the vertebra and the relative roles of the cortical and trabecular bone. Moreover, this work provided an important mechanistic link between vertebral strength, endplate failure, and the material behavior of the intervertebral disc. From a clinical perspective, the results of this research have provided relevant, new insight regarding microarchitecture assessment of vertebral strength and diagnosis of vertebral fractures.

Combining the latest advances in micro-CT imaging, high-resolution finite element modeling, and biomechanical testing, we compared for the first time the relative roles of the cortical shell and trabecular microarchitecture in explaining variations in whole-vertebral strength, stiffness, and load sharing (Chapter two). Whereas previous work quantified the relative load-carrying capacities of the cortical shell and trabecular bone [48, 49, 72], the extent to which variations in these compartments were associated with variations in vertebral strength across individuals was unknown. We found that variation in trabecular microarchitecture was highly associated with vertebral strength and that its role was mediated by bone mass and density but not by cross-sectional area or the cortical shell. For example, variation in structural model index (SMI) and trabecular thickness (Tb.Th) together explained ~75% of the observed variations in vertebral strength. However, there were significant cross-correlations between these trabecular microarchitecture parameters and bone mass and density, and thus, different parameters were important predictors after accounting for variations in vertebral strength due to bone mass and density first. In that case, only the degree of anisotropy (DA) of the trabecular bone had a significant (but small) role. This suggests that the traditional trabecular microarchitecture parameters may have a limited ability to improve vertebral strength prediction and clinical fracture risk assessment beyond the current measures of bone mineral density.

In Chapter three, the individual trabeculae within the vertebrae were classified by their anatomical orientation, and a combination of high-resolution finite element analysis and biomechanical testing was used to study the influence of trabeculae in different orientations on vertebral strength. Not only did the finite element analyses provide mechanistic insight into the results from the biomechanical tests, but they also led to the development of a new, biomechanics-based predictor of vertebral strength. The results from Chapter three demonstrated that variation in vertebral strength across individuals was primarily due to variation in the bone volume fraction of the vertical trabeculae. This is because the major load paths were parallel columns of vertically-oriented bone—the vertical trabeculae and the cortical shell. Whereas variations in the amount of vertical trabeculae had an important role in vertebral strength, variations in the amount of cortical tissue had a minor role. A new microarchitecture parameter, the vertical tissue fraction, was developed to reflect these findings. Unlike the microarchitecture parameters evaluated in the previous chapter, the vertical tissue fraction was nearly independent of bone density and was a significant predictor of vertebral strength before and after accounting for the variation in vertebral strength due to variation in bone density. From a biomechanical

perspective, this new parameter represents an aspect of trabecular microarchitecture with the greatest potential for non-invasive, microarchitecture analysis of vertebral strength.

The research presented in Chapter three represents a novel approach to the "weakest link" concept: high-resolution finite element analysis is first used to identify the structures with the highest stress, *i.e.* the weakest links in the vertebrae, morphological analysis is used to characterize the inter-individual variation in certain aspects of those structures, and biomechanical testing is used to assess the predictive ability. Although this systematic method of identifying the structural determinants of bone strength was only applied to a single loading condition in the vertebra, the method should also apply generally to more complex loading conditions and to bone strength at other anatomic sites (*e.g.* proximal femur).

In Chapter four, the biomechanical mechanisms of vertebral strength were studied in a cohort of elderly vertebrae. This study is the first to apply high-resolution finite element modeling with geometric and material nonlinearities to whole bones. Thus, whereas previous work using linear analysis was limited to the behavior of the vertebra under small loads, the research in this chapter using nonlinear analysis provided new insight into the behavior of the vertebra in response to an isolated overload. Due to the variations in failure mechanisms between porous and dense vertebrae, significantly less tissue yielding accompanied an overload of the more porous vertebrae than the more dense vertebrae, illustrating a new aspect of vertebral fragility: as bone volume fraction (density) decreases with aging and disease, not only is the vertebra becoming weaker, but it is also becoming much less structurally robust. The findings could help explain why overloads tend to cause greater strength reductions in low-density vertebrae [102] and may also have clinical implications in terms of the associated bone remodeling response and the effects of treatment.

The results from the research combining high-resolution finite element modeling with cadaver biomechanical testing (Chapters 2-4) have practical implications regarding the relative importance of cortical *vs.* trabecular bone for *in vivo*, microarchitecture analysis of vertebral strength and fracture risk. Although the cortical shell has a substantial load-bearing role in the vertebra [48, 49, 73, 98, 113], new findings from this dissertation indicated that variations in cortical thickness and the relative mass of the cortical shell were small and were only weakly associated with variations in vertebral strength across individuals. Our findings also indicated that the role of trabecular microarchitecture was mediated by bone mass and density. *In vivo*, microarchitecture assessment of vertebral strength and fracture risk should therefore focus on the aspects of the vertebral microarchitecture that satisfy three criteria: 1) They are important from a biomechanical perspective, *i.e.* they reflect the biomechanical behavior of the vertebra; 2) They exhibit wide variations across individuals; *and* 3) They are significant predictors of vertebral strength even after adjusting for bone density. In light of these findings, we suggested a new microarchitectural determinant of vertebral strength that satisfies these criteria: vertical tissue fraction. Apart from the clinical significance of these findings, the analysis of the deformation and failure mechanisms in the vertebra is an important step in understanding the etiology of vertebral fractures.

Chapter five focused on the mechanisms of initial endplate failure. Despite their frequent involvement in osteoporotic vertebral fractures [61-64, 150, 151], the mechanisms underlying

endplate failure were unclear. A detailed investigation into this issue revealed two striking characteristics of the endplates that help to explain their frequent involvement in osteoporotic vertebral fractures: the endplates are at the highest risk of initial failure due to the development of high tensile strains, and the development of such high tensile strains is directly associated with the material behavior of the intervertebral disc. The tension that develops in the plane of the endplates is notable not only because bone tissue is weaker in tension than in compression, but also because the type of tension in the endplates—*biaxial* tension—is particularly aggressive compared to *uniaxial* tension which occurs elsewhere (and less frequently) in the vertebra. Together, these findings support the concept that endplate failure may be an etiologic factor in osteoporotic vertebral fracture and that radiological evidence of changes in the endplates should be an essential part of the definition of vertebral fracture [36]. In a previous study which observed frequent endplate failures during cadaver experiments, variations in disc properties explained a remarkable 70% of the variations in vertebral strength [25], but the link between the variations in disc properties and the mechanism of endplate or vertebral failure was unclear. Eswaran *et al.* predicted that the endplates were highly strained [72], although the neither the relative magnitude of the strains nor the type of the strains (*i.e.* tension *vs.* compression) in the vertebra was compared, so the importance of the high endplate strains was unknown. The new data in this dissertation thus provide a mechanistic link between endplate failure, initial vertebral failure, and the material behavior of the intervertebral disc. One key challenge for spine researchers will be to measure intra- and inter-individual variations in disc material behavior and to determine the effect of these variations on endplate failure mechanisms. The techniques described in this research combined with biomechanical testing of the intervertebral disc should provide new and important insight into the biomechanical interaction between the endplates and the intervertebral disc.

There are several strengths of this research. First, this research used both high-resolution finite element modeling and biomechanical testing in order to exploit the unique capabilities of each technique. This combined approach provided mechanistic insight into whole vertebral biomechanical behavior, a feature that differentiates the research from recent work that considered only statistical correlations when studying structure-function relationships in the whole vertebra [25, 121, 128]. Second, we studied multiple vertebrae exhibiting a wide range of bone morphologies, thereby accounting for biological heterogeneity and providing a reasonable degree of external validity to the results. Third, the fully nonlinear analysis of whole vertebrae (up to 1.5 billion degrees of freedom) incorporating the latest advances in efficient solver algorithms [88] and state-of-the-art supercomputing technology places this research at the forefront of current efforts in computational bone mechanics. Fourth, we performed high-resolution micro-CT imaging (30 μm spatial resolution) to reduce partial volume effects on the accuracy of microarchitecture measurements [106] and utilized a novel method for characterizing the morphology of individual trabeculae [118]. Related to this, a notable feature in the analysis of trabeculae with various orientations was the use of finite element models with and without the cortical shell, a unique advantage of using high-resolution computational analysis. Removing the thin cortical shell enabled us to test the hypothesis that the effects of the vertical trabeculae on vertebral stiffness were independent of the cortical shell and its variations. This approach may be especially important for future studies investigating the response of the

vertebra to forward flexion—a loading mode where the shell is thought to play a greater role [109].

There are two areas of future research necessary to further extend the relevance of the work presented in this dissertation. The first area is associated with nonlinear finite element analysis of whole bones. The current findings are limited to vertebral behavior up to the point of apparent yielding; however, the post-yield and ultimate behavior of vertebra is also relevant. Modification of the tissue constitutive model to include damage or softening behavior is recommended for predicting post-yield behavior [147]. Changes in the current modeling approach related to thresholding are also recommended to improve the accuracy of vertebral strength predictions, since subtle differences in thresholding can result in substantial errors in micro-CT-derived mechanical properties [68], and because there is currently no objective way of thresholding images of whole bones. Finally, this dissertation only focused on uniform compressive loading. Since many osteoporotic vertebral fractures are anterior wedge fractures [34], the response to combined compression and anterior bending is a topic of clinical interest requiring additional work.

The second area of future research is motivated by the study that investigated the mechanisms of initial endplate failure (Chapter 5). The endplates are an understudied anatomical region and are rich for future scientific discovery since the biomechanical interaction between the endplates and the intervertebral disc is critical with respect to both vertebral fractures and discogenic back pain. In terms of vertebral fractures, establishing the endplates' general dependence on the material behavior of the intervertebral disc motivates future work to assess specific variations in disc behavior concomitant with disc degeneration and the mechanisms of influence on vertebral strength. In terms of discogenic back pain, the biological implication of high tensile strains in the endplates is unclear at this point and requires future study. For example, the effect of high tensile strains on the permeability of the endplates is unknown. Endplate permeability is thought to be a critical regulator of intervertebral disc health. If high tensile strains lead to a biological response that reduces endplate permeability, then this could be an important cause of disc degeneration and source of back pain. However, little is known about the relationship between the biomechanical behavior of the endplates and endplate permeability—or about the interaction between the endplates and the intervertebral disc in general—and thus, this is an exciting topic for future work.

In closure, this research answers fundamental questions regarding the role of trabecular microarchitecture in explaining the observed variations in vertebral strength across individuals, and provides new insight into the etiology of age-related vertebral fractures. The studies on trabecular microarchitecture (Chapters two and three) identified a novel, biomechanics-based determinant of vertebral strength. The studies on failure mechanisms and fracture etiology (Chapters four and five, respectively) illustrated a new aspect of vertebral fragility and a mechanistic link between the failure mechanisms of the vertebra and the material behavior of the intervertebral disc. This dissertation also outlines areas of research to further advance our understanding of vertebral fracture etiology and describes a systematic approach for identifying micoarchitectural determinants of bone strength that could be used at other anatomic sites.

7. APPENDIX

7.1 Influence of element size on predictions of vertebral strength and tissue yielding using high-resolution finite element analysis with geometric and material nonlinearities

To verify the accuracy of our reported trends for tissue yielding, we performed a convergence study comparing 30 μm-resolution meshes to 60 μm-resolution meshes. Five vertebrae ranging in BV/TV from 0.08 to 0.19 were selected. Using fully nonlinear finite element analyses, the apparent yield strength and the percentage of yielded tissue were compared between the 30 μm and 60 μm models. The largest of these models contained up to 1.6 billion degrees of freedom and required over 135,000 hours of CPU time.

Compared to the 30 μm models, the 60 μm models over-predicted yield strength ($p < 0.01$ paired *t*-test) and the percentage of yielded tissue ($p < 0.05$ paired *t*-test) but the effect was constant (30 μm *vs*. 60 μm yield strength: slope = 0.95, offset = 0; 30 μm *vs.* 60 μm yielded tissue: slope = 0.88, offset = 0; $r^2 = 0.99$ for both outcomes). Based on these results, we conclude that the finite element models with 60 μm element size accurately capture the inter-specimen variations in yield strength and in the amount of yielded tissue; thus, using the models with this larger element size should not alter our conclusions.

7.2 Validity of predictions of vertebral strength from high-resolution finite element analysis with geometric and material nonlinearities

To assess model validity, finite element predictions of the apparent yield strength were compared with measurements of vertebral strength from a corresponding series of biomechanical experiments. Details of the biomechanical experiments are described elsewhere [23, 77, 102]. Briefly, the vertebral bodies were placed between PMMA endcaps and compressed in displacement control at a slow strain rate (0.05-0.5% strain/s) after cyclic preconditioning. Vertebral strength was defined as the peak force achieved during the loading cycle.

The fully nonlinear finite element analyses accurately predicted variations in measured vertebral strength. Predicted yield strength explained 85% of the variations in measured vertebral strength for the same vertebrae ($p < 0.0001$, Figure 7-1), indicating the overall validity of the models was good. Variation in vertebral strength was also highly associated ($r^2 = 0.79$) with variations in finite element-predicted stiffness ($p < 0.0001$). Despite the high correlation between finite element-derived measures of strength and stiffness ($r^2 = 0.99$), the residuals from predicted strength using the finite element-derived yield strength as the predictor (absolute residual = 0.4 ± 0.3 kN) were 20% lower, on average ($p < 0.01$, paired *t*-test), than the residuals from predicted strength using the finite element-derived stiffness as the predictor (0.5 ± 0.4 kN).

7.3 Effects of disc properties on endplate deformation and failure mechanisms

To further understand the effect of Poisson-type expansion of the disc on the stresses in the endplates, we analyzed the stress state within a small region of the superior endplate of each vertebra. A 1 mm x 1 mm transverse region of interest was defined through the thickness of the central endplate (Figure 7-2A). The bone in this location had the greatest concentration of highly-strained tissue and its orientation was approximately coplanar with respect to both the

local x-y plane and the transverse anatomical plane. For each vertebra, the average stress at every inferior-superior position in the region of interest was normalized by the maximum stress in that region of interest. The mean value of the normalized stress at each inferior-superior position was then computed for all vertebrae. While the deformation of a beam is exemplified by a stress profile that varies linearly through the thickness of the beam (Figure 7-2B), stress profiles in the anterior-posterior and medial-lateral directions (Figure 7-2C and Figure 7-2D, respectively) indicated the presence of tensile stresses throughout the thickness of the endplates in both directions. This in-plane biaxial tension through the thickness of the endplate is more consistent with the stretching of a membrane (Figure 7-2B). However, suppressing the Poisson expansion of the disc mitigated the tensile stresses in the anterior-posterior and medial-lateral directions in the regions of interest (Figure 7-2C and Figure 7-2D, respectively, and Table 7-1). Taken together, these results suggest that the endplates both stretch and bend under applied compressive loads and that a state of biaxial tension arises due to the Poisson expansion of the intervertebral disc.

Table 7-1: Effect of suppressing the Poisson expansion of the disc on the in-plane stress components within the region of interest of the superior endplate.

	With Poisson expansion	Without Poisson expansion
Anterior-posterior stress, σ_x (MPa)	3.93 ± 1.81	0.32 ± 0.40
Medial-lateral stress, σ_y (MPa)	2.81 ± 1.53	-0.10 ± 0.28
Maximum principal stress, σ_1 (MPa)	5.76 ± 1.52	0.80 ± 0.70
Minimum principal stress, σ_2 (MPa)	0.98 ± 1.97	-0.58 ± 0.69
Maximum shear stress, τ_{max} (MPa)	2.39 ± 0.94	0.69 ± 0.63
Principal angle*, θ (degrees)	1.01 ± 6.61	2.87 ± 10.23

Data given as mean ± SD (n = 22 vertebral bodies)
* Angle measured clockwise with respect to x-y coordinate system shown in Figure 7-2
All comparisons were statistically significant ($p < 0.0001$, paired t-test) except for the effect of suppressing the Poisson expansion on the principal angle

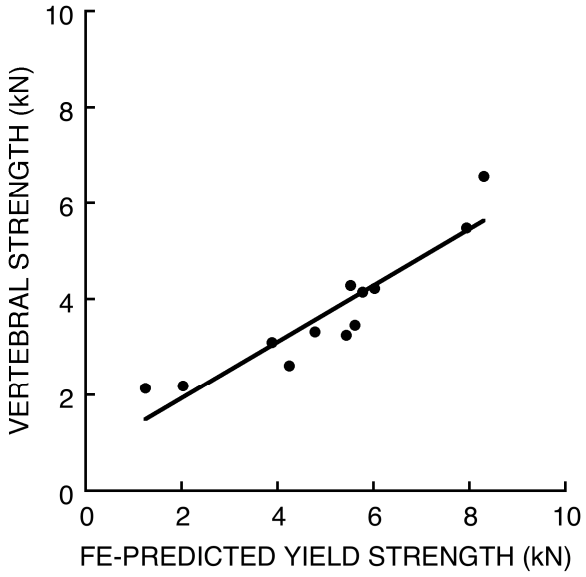

Figure 7-1: Variations in experiment-measured vertebral strength were highly associated ($r^2 = 0.85$) with variations in finite element-predicted yield strength.

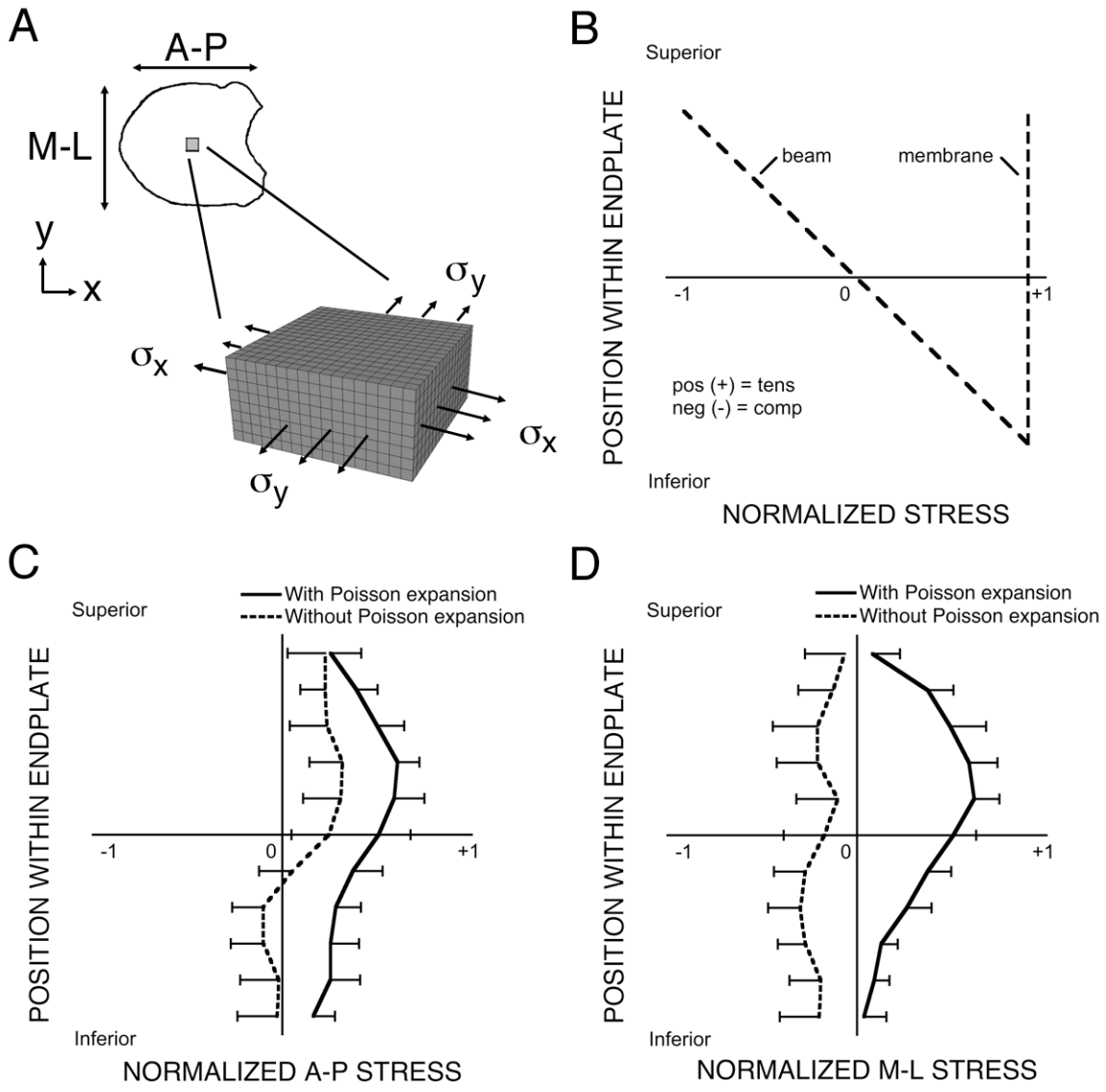

Figure 7-2: (A) Illustration of a transverse region of interest (1 mm x 1 mm) through the thickness of the superior endplate. The top and bottom surfaces of the region of interest represent the superior and inferior surfaces of the endplate, respectively. (B) Theoretical stress profiles in regions of interest deforming like a beam and like a membrane. The location of the neutral axis is indicated by the position of the horizontal axis. (C) Effect of suppressing the Poisson expansion of the disc on anterior-posterior (A-P) stress profiles within the region of interest. The mean stress in the models loaded via discs with Poisson expansion was greater than the mean stress in the models loaded via discs without this behavior ($p < 0.05$, paired *t*-test) at all inferior-superior locations within the region of interest except for the superior surface ($p = 0.63$), and was significantly different than zero ($p < 0.01$) at all inferior-superior locations. (D) Effect of suppressing the Poisson expansion of the disc on medial-lateral (M-L) stress profiles within the region of interest. The mean stress in the models loaded via discs with Poisson expansion was greater than the mean stress in the models loaded via discs without this behavior ($p < 0.01$, paired *t*-test) at all inferior-superior locations within the region of interest except for the superior surface ($p = 0.06$), and was significantly different than zero ($p < 0.05$) at all inferior-superior locations except for the top and bottom surfaces. Error bars show 95% CI ($n = 22$ vertebral bodies).

8. REFERENCES

[1] Riggs BL, Melton LJ. The Worldwide Problem of Osteoporosis - Insights Afforded by Epidemiology. Bone 1995;17: S505-S511.

[2] Kanis JA, Melton LJ, Christiansen C, Johnston CC, Khaltaev N. The diagnosis of osteoporosis. J Bone Miner Res 1994;9: 1137-1141.

[3] Cummings SR, Bates D, Black DM. Clinical use of bone densitometry - Scientific review. JAMA 2002;288: 1889-1897.

[4] Guglielmi G, Gluer CC, Majumdar S, Blunt BA, Genant HK. Current methods and advances in bone densitometry. Eur Radiol 1995;5: 129-39.

[5] Schuit SC, van der Klift M, Weel AE, de Laet CE, Burger H, Seeman E, Hofman A, Uitterlinden AG, van Leeuwen JP, Pols HA. Fracture incidence and association with bone mineral density in elderly men and women: the Rotterdam Study. Bone 2004;34: 195-202.

[6] Cummings SR. How drugs decrease fracture risk: lessons from trials. J Musculoskelet Neuronal Interact 2002;2: 198-200.

[7] Cummings SR, Karpf DB, Harris F, Genant HK, Ensrud K, LaCroix AZ, Black DM. Improvement in spine bone density and reduction in risk of vertebral fractures during treatment with antiresorptive drugs. Am J Med 2002;112: 281-289.

[8] Delmas PD. How does antiresorptive therapy decrease the risk of fracture in women with osteoporosis? Bone 2000;27: 1-3.

[9] Delmas PD, Seeman E. Changes in bone mineral density explain little of the reduction in vertebral or nonvertebral fracture risk with anti-resorptive therapy. Bone 2004;34: 599-604.

[10] Kanis JA, Borgstrom F, De Laet C, Johansson H, Johnell O, Jonsson B, Oden A, Zethraeus N, Pfleger B, Khaltaev N. Assessment of fracture risk. Osteoporos Int 2005;16: 581-9.

[11] Bartel DL, Davy DT, Keaveny TM. Orthopaedic biomechanics - Mechanics and design in musculoskeletal systems. Upper Saddle River, NJ: Pearson/Prentice Hall; 2006.

[12] Malone AM, Anderson CT, Tummala P, Kwon RY, Johnston TR, Stearns T, Jacobs CR. Primary cilia mediate mechanosensing in bone cells by a calcium-independent mechanism. Proc Natl Acad Sci U S A 2007;104: 13325-30.

[13] Taylor AF, Saunders MM, Shingle DL, Cimbala JM, Zhou Z, Donahue HJ. Mechanically stimulated osteocytes regulate osteoblastic activity via gap junctions. Am J Physiol Cell Physiol 2007;292: C545-52.

[14] Keaveny TM, Buckley JM. Biomechanics of vertebral bone. In: Kurtz SM, Edidin AA, editors. Spine technology handbook. New York: Academic Press; 2006.

[15] Ohshima H, Tsuji H, Hirano N, Ishihara H, Katoh Y, Yamada H. Water diffusion pathway, swelling pressure, and biomechanical properties of the intervertebral disc during compression load. Spine 1989;14: 1234-44.

[16] Edwards WT, Zheng YG, Ferrara LA, Yuan HA. Structural features and thickness of the vertebral cortex in the thoracolumbar spine. Spine 2001;26: 218-225.

[17] Silva MJ, Wang C, Keaveny TM, Hayes WC. Direct and computed-tomography thickness measurements of the human lumbar vertebral shell and end-plate. Bone 1994;15: 409-414.

[18] Mosekilde L, Raisz, Reeve, Malluche, Snyder. Vertebral structure and strength in-vivo and in-vitro. Calcif Tissue Int 1993;53: S121-S126.

[19] Roy ME, Rho JY, Tsui TY, Evans ND, Pharr GM. Mechanical and morphological variation of the human lumbar vertebral cortical and trabecular bone. J Biomed Mater Res 1999;44: 191-197.

[20] Zhao FD, Pollintine P, Hole BD, Adams MA, Dolan P. Vertebral fractures usually affect the cranial endplate because it is thinner and supported by less-dense trabecular bone. Bone 2009;44: 372-9.

[21] Ritzel H, Amling M, Posl M, Hahn M, Delling G. The thickness of human vertebral cortical bone and its changes in aging and osteoporosis: A histomorphometric analysis of the complete spinal column from thirty-seven autopsy specimens. J Bone Miner Res 1997;12: 89-95.

[22] Vesterby A, Mosekilde L, Gundersen HJG, Melsen F, Mosekilde L, Holem K, Sorensen S. Biologically meaningful determinants of the in vitro strength of lumbar vertebrae. Bone 1991;12: 219-224.

[23] Fields AJ, Eswaran SK, Jekir MG, Keaveny TM. Role of trabecular microarchitecture in whole-verterbal body biomechanical behavior. J Bone Miner Res 2009;29: 1523-30.

[24] Cody DD, Goldstein SA, Flynn MJ, Brown EB. Correlations between vertebral regional bone-mineral density (RBMD) and whole-bone fracture load. Spine 1991;16: 146-154.

[25] Hulme PA, Boyd SK, Ferguson SJ. Regional variation in vertebral bone morphology and its contribution to vertebral fracture strength. Bone 2007;41: 946-57.

[26] Keller TS, Hansson TH, Abram AC, Spengler DM, Panjabi MM. Regional variations in the compressive properties of lumbar vertebral trabeculae - effects of disk degeneration. Spine 1989;14: 1012-1019.

[27] Edmondston SJ, Singer KP, Day RE, Price RI, Breidahl PD. Ex vivo estimation of thoracolumbar vertebral body compressive strength: the relative contributions of bone densitometry and vertebral morphometry. Osteoporos Int 1997;7: 142-8.

[28] Singer K, Edmondston S, Day R, Breidahl P, Price R. Prediction of thoracic and lumbar vertebral body compressive strength - correlations with bone-mineral density and vertebral region. Bone 1995;17: 167-174.

[29] Adams MA, Hutton WC. The mechanical function of the lumbar apophyseal joints. Spine 1983;8: 327-30.

[30] Grisso JA, Kelsey JL, Strom BL, Chiu GY, Maislin G, O'Brien LA, Hoffman S, Kaplan F. Risk factors for falls as a cause of hip fracture in women. The Northeast Hip Fracture Study Group. N Engl J Med 1991;324: 1326-31.

[31] Michelson JD, Myers A, Jinnah R, Cox Q, Van Natta M. Epidemiology of hip fractures among the elderly. Risk factors for fracture type. Clin Orthop Relat Res 1995: 129-35.

[32] Cooper C, Atkinson EJ, O'Fallon WM, Melton LJ. Incidence of clinically diagnosed vertebral fractures: a population-based study in Rochester, Minnesota, 1985-1989. J Bone Miner Res 1992;7: 221-227.

[33] Myers ER, Wilson SE, Greenspan SL. Vertebral fractures in the elderly occur with falling and bending. Journal of Bone and Mineral Research 1996;11: S355.

[34] Eastell R, Cedel SL, Wahner HW, Riggs BL, Melton LJ. Classification of vertebral fractures. J Bone Miner Res 1991;6: 207-215.

[35] Genant HK, Cooper C, Poor G, Reid I, Ehrlich G, Kanis J, Nordin BE, Barrett-Connor E, Black D, Bonjour JP, Dawson-Hughes B, Delmas PD, Dequeker J, Ragi Eis S, Gennari C, Johnell O, Johnston CC, Jr., Lau EM, Liberman UA, Lindsay R, Martin TJ, Masri B, Mautalen CA, Meunier PJ, Khaltaev N, et al. Interim report and recommendations of the World Health Organization Task-Force for Osteoporosis. Osteoporos Int 1999;10: 259-64.

[36] Ferrar L, Jiang G, Adams J, Eastell R. Identification of vertebral fractures: An update. Osteoporos Int 2005;16: 717-728.

[37] Mosekilde L, Mosekilde L. Normal vertebral body size and compressive strength: relations to age and to vertebral and iliac trabecular bone compressive strength. Bone 1986;7: 207-212.

[38] Mosekilde L, Mosekilde L. Sex differences in age-related changes in vertebral body size, density and biomechanical competence in normal individuals. Bone 1990;11: 67-73.

[39] Antonacci MD, Hanson DS, Leblanc A, Heggeness MH. Regional variation in vertebral bone density and trabecular architecture are influenced by osteoarthritic change and osteoporosis. Spine 1997;22: 2393-401; discussion 2401-2.

[40] Bell GH, Dunbar O, Beck JS, Gibb A. Variations in strength of vertebrae with age and their relation to osteoporosis. Calcif Tissue Res 1967;1: 75-86.

[41] Snyder BD, Piazza S, Edwards WT, Hayes WC. Role of trabecular morphology in the etiology of age-related vertebral fractures. Calcif Tissue Int 1993;53S: S14-S22.

[42] Nazarian A, Müller R. Time-lapsed microstructural imaging of bone failure behavior. J Biomech 2004;37: 55-65.

[43] Bevill G, Eswaran SK, Gupta A, Papadopoulos P, Keaveny TM. Influence of bone volume fraction and architecture on computed large-deformation failure mechanisms in human trabecular bone. Bone 2006;39: 1218-25.

[44] Bevill G, Farhamand F, Keaveny TM. Heterogeneity of yield strain in low-density versus high-density human trabecular bone. J Biomech 2009;42: 2165-70.

[45] Morgan EF, Bayraktar HH, Yeh OC, Majumdar S, Burghardt A, Keaveny TM. Contribution of inter-site variations in architecture to trabecular bone apparent yield strains. J Biomech 2004;37: 1413-20.

[46] Ito M, Ikeda K, Nishiguchi M, Shindo H, Uetani M, Hosoi T, Orimo H. Multi-detector row CT imaging of vertebral microstructure for evaluation of fracture risk. J Bone Miner Res 2005;20: 1828-36.

[47] Sornay-Rendu E, Boutroy S, Munoz F, Delmas PD. Alterations of cortical and trabecular architecture are associated with fractures in postmenopausal women, partially independent of decreased BMD measured by DXA: the OFELY study. J Bone Miner Res 2007;22: 425-33.

[48] Eswaran SK, Bayraktar HH, Adams MF, Gupta A, Hoffman PF, Lee DC, Papadopoulos P, Keaveny TM. The micro-mechanics of cortical shell removal in the human vertebral body. Comput Method Appl Mech Eng 2007;196: 3025-32.

[49] Eswaran SK, Gupta A, Adams MF, Keaveny TM. Cortical and trabecular load sharing in the human vertebral body. J Bone Miner Res 2006;21: 307-14.

[50] Mcbroom RJ, Hayes WC, Edwards WT, Goldberg RP, White AA. Prediction of vertebral body compressive fracture using quantitative computed-tomography. J Bone Joint Surg Am 1985;67A: 1206-1214.

[51] Rockoff SD, Sweet E, Bleustein J. The relative contribution of trabecular and cortical bone to the strength of human lumbar vertebrae. Calcif Tissue Res 1969;3: 163-175.

[52] Adams MA, McNally DS, Dolan P. 'Stress' distributions inside intervertebral discs. The effects of age and degeneration. J Bone Joint Surg Br 1996;78: 965-72.

[53] Middleditch A, J. O. Functional Anatomy of the Spine. 2nd ed. Boston: Elsevier Ltd.; 2005.

[54] Bay BK, Yerby SA, McLain RF, Toh E. Measurement of strain distributions within vertebral body sections by texture correlation. Spine 1999;24: 10-17.

[55] Hansson T, Roos B. The relation between bone-mineral content, experimental compression fractures, and disk degeneration in lumbar vertebrae. Spine 1981;6: 147-153.

[56] Kurowski P, Kubo A. The relationship of degeneration of the intervertebral disc to mechanical loading conditions on lumbar vertebrae. Spine 1986;11: 726-731.

[57] Shirazi-Adl SA, Shrivastava SC, Ahmed AM. Stress analysis of the lumbar disc-body unit in compression: A three-dimensional nonlinear finite element study. Spine 1984;9: 120-134.

[58] Antoniou J, Steffen T, Nelson F, Winterbottom N, Hollander AP, Poole RA, Aebi M, Alini M. The human lumbar intervertebral disc: evidence for changes in the biosynthesis and denaturation of the extracellular matrix with growth, maturation, ageing, and degeneration. J Clin Invest 1996;98: 996-1003.

[59] Iatridis JC, Setton LA, Weidenbaum M, Mow VC. Alterations in the mechanical behavior of the human lumbar nucleus pulposus with degeneration and aging. J Orthop Res 1997;15: 318-22.

[60] Homminga J, Weinans H, Gowin W, Felsenberg D, Huiskes R. Osteoporosis changes the amount of vertebral trabecular bone at risk of fracture but not the vertebral load distribution. Spine 2001;26: 1555-61.

[61] Aebi M. Classification of thoracolumbar fractures and dislocations. Eur Spine J 2009.

[62] Brinckmann P, Frobin W, Hierholzer E, Horst M. Deformation of the vertebral end-plate under axial loading of the spine. Spine 1983;8: 851-6.

[63] Moore RJ. The vertebral end-plate: what do we know? Eur Spine J 2000;9: 92-6.

[64] Wasnich RD. Vertebral fracture epidemiology. Bone 1996;18: 179S-183S.

[65] Hildebrand T, Laib A, Müller R, Dequeker J, Rüegsegger P. Direct three-dimensional morphometric analysis of human cancellous bone: microstructural data from spine, femur, iliac crest, and calcaneus. J Bone Miner Res 1999;14: 1167-74.

[66] Odgaard A, Gundersen HJ. Quantification of connectivity in cancellous bone, with special emphasis on 3-D reconstructions. Bone 1993;14: 173-82.

[67] Ulrich D, van Rietbergen B, Laib A, Ruegsegger P. The ability of three-dimensional structural indices to reflect mechanical aspects of trabecular bone. Bone 1999;25: 55-60.

[68] Bevill G, Eswaran SK, Farahmand F, Keaveny TM. The influence of boundary conditions and loading mode on high-resolution finite element-computed trabecular tissue properties. Bone 2009;44: 573-8.

[69] Bourne BC, van der Meulen MC. Finite element models predict cancellous apparent modulus when tissue modulus is scaled from specimen CT-attenuation. J Biomech 2004;37: 613-21.

[70] Easley SK, Jekir MG, Burghardt AJ, Li M, Keaveny TM. Contribution of the intra-specimen variations in tissue mineralization to PTH- and raloxifene-induced changes in stiffness of rat vertebrae. Bone 2010;46: 1162-9.

[71] Jaasma MJ, Bayraktar HH, Niebur GL, Keaveny TM. Biomechanical effects of intraspecimen variations in tissue modulus for trabecular bone. J Biomech 2002;35: 237-246.

[72] Eswaran SK, Gupta A, Keaveny TM. Locations of bone tissue at high risk of initial failure during compressive loading of the human vertebral body. Bone 2007;41: 733-9.

[73] Homminga J, Van-Rietbergen B, Lochmüller EM, Weinans H, Eckstein F, Huiskes R. The osteoporotic vertebral structure is well adapted to the loads of daily life, but not to infrequent "error" loads. Bone 2004;34: 510-6.

[74] Frei H, Oxland TR, Nolte LP. Thoracolumbar spine mechanics contrasted under compression and shear loading. J Orthop Res 2002;20: 1333-8.

[75] Bayraktar HH, Morgan EF, Niebur GL, Morris GE, Wong EK, Keaveny TM. Comparison of the elastic and yield properties of human femoral trabecular and cortical bone tissue. J Biomech 2004;37: 27-35.

[76] Van Rietbergen B, Weinans H, Huiskes R, Odgaard A. A new method to determine trabecular bone elastic properties and loading using micromechanical finite element models. J Biomech 1995;28: 69-81.

[77] Buckley JM, Loo K, Motherway J. Comparison of quantitative computed tomography-based measures in predicting vertebral compressive strength. Bone 2007;40: 767-74.

[78] Chevalier Y, Charlebois M, Pahra D, Varga P, Heini P, Schneider E, Zysset P. A patient-specific finite element methodology to predict damage accumulation in vertebral bodies under axial compression, sagittal flexion and combined loads. Comput Methods Biomech Biomed Engin 2008;11: 477-87.

[79] Crawford RP, Cann CE, Keaveny TM. Finite element models predict in vitro vertebral body compressive strength better than quantitative computed tomography. Bone 2003;33: 744-50.

[80] Faulkner KG, Cann CE, Hasegawa BH. Effect of bone distribution on vertebral strength: assessment with patient-specific nonlinear finite element analysis. Radiology 1991;179: 669-74.

[81] Graeff C, Chevalier Y, Charlebois M, Varga P, Pahr D, Nickelsen TN, Morlock MM, Gluer CC, Zysset PK. Improvements in vertebral body strength under teriparatide treatment

assessed in vivo by finite element analysis: results from the EUROFORS study. J Bone Miner Res 2009;24: 1672-80.

[82] Melton LJ, 3rd, Riggs BL, Keaveny TM, Achenbach SJ, Hoffmann PF, Camp JJ, Rouleau PA, Bouxsein ML, Amin S, Atkinson EJ, Robb RA, Khosla S. Structural determinants of vertebral fracture risk. J Bone Miner Res 2007;22: 1885-92.

[83] Hou FJ, Lang SM, Hoshaw SJ, Reimann DA, Fyhrie DP. Human vertebral body apparent and hard tissue stiffness. J Biomech 1998;31: 1009-15.

[84] Kabel J, van Rietbergen B, Dalstra M, Odgaard A, Huiskes R. The role of an effective isotropic tissue modulus in the elastic properties of cancellous bone. J Biomech 1999;32: 673-80.

[85] Nagaraja S, Couse TL, Guldberg RE. Trabecular bone microdamage and microstructural stresses under uniaxial compression. J Biomech 2005;38: 707-16.

[86] Niebur GL, Feldstein MJ, Yuen JC, Chen TJ, Keaveny TM. High-resolution finite element models with tissue strength asymmetry accurately predict failure of trabecular bone. J Biomech 2000;33: 1575-1583.

[87] Shi X, Liu XS, Wang X, Guo XE, Niebur GL. Effects of trabecular type and orientation on microdamage susceptibility in trabecular bone. Bone 2010;46: 1260-6.

[88] Adams MF, Bayraktar HH, Keaveny TM, Papadopoulos P. Ultrascalable implicit finite element analyses in solid mechanics with over a half a billion degrees of freedom. In: ACM/IEEE Proceedings of SC2004: High Performance Networking and Computing; 2004.

[89] Arbenz P, van Lenthe GH, Mennel U, Müller R, Sala M. A scalable multi-level preconditioner for matrix-free μ-finite element analysis of human bone structures. Int J Num Meth Engg 2008;73: 927-47.

[90] Stölken JS, Kinney JH. On the importance of geometric nonlinearity in finite-element simulations of trabecular bone failure. Bone 2003;33: 494-504.

[91] Keaveny TM. Strength of trabecular bone. In: Cowin SC, editor. Bone mechanics handbook. Boc Raton, Fl: CRC press; 2001, p. **16**-1-42.

[92] Heaney RP. Is the paradigm shifting? Bone 2003;33: 457-65.

[93] Hernandez CJ, Keaveny TM. A biomechanical perspective on bone quality. Bone 2006;39: 1173-81.

[94] Goulet RW, Goldstein SA, Ciarelli MJ, Kuhn JL, Brown MB, Feldkamp LA. The relationship between the structural and orthogonal compressive properties of trabecular bone. J Biomech 1994;27: 375-389.

[95] Newitt DC, Majumdar S, van Rietbergen B, von Ingersleben G, Harris ST, Genant HK, Chesnut C, Garnero P, MacDonald B. In vivo assessment of architecture and micro-finite element analysis derived indices of mechanical properties of trabecular bone in the radius. Osteoporos Int 2002;13: 6-17.

[96] Ebbesen EN, Thomsen JS, Beck-Nielsen H, Nepper-Rasmussen HJ, Mosekilde L. Lumbar vertebral body compressive strength evaluated by dual-energy X-ray absorptiometry, quantitative computed tomography, and ashing. Bone 1999;25: 713-24.

[97] Banse X, Devogelaer JP, Munting E, Delloye C, Cornu O, Grynpas M. Inhomogeneity of human vertebral cancellous bone: systematic density and structure patterns inside the vertebral body. Bone 2001;28: 563-71.

[98] Andresen R, Werner HJ, Schober HC. Contribution of the cortical shell of vertebrae to mechanical behaviour of the lumbar vertebrae with implications for predicting fracture risk. Brit J Radiol 1998;71: 759-65.

[99] Morgan EF, Bayraktar HH, Keaveny TM. Trabecular bone modulus-density relationships depend on anatomic site. J Biomech 2003;36: 897-904.

[100] Müller R, Hannan M, Smith SY, Bauss F. Intermittent ibandronate preserves bone quality and bone strength in the lumbar spine after 16 months of treatment in the ovariectomized cynomolgus monkey. J Bone Miner Res 2004;19: 1787-96.

[101] Eriksson SAV, Isberg BO, Lindgren JU. Prediction of vertebral strength by dual photon-absorptiometry and quantitative computed-tomography. Calcif Tissue Int 1989;44: 243-250.

[102] Kopperdahl DL, Pearlman JL, Keaveny TM. Biomechanical consequences of an isolated overload on the human vertebral body. J Orthop Res 2000;18: 685-690.

[103] Carter DR, Hayes WC. The compressive behavior of bone as a two-phase porous structure. J Bone Joint Surg Am 1977;59-A: 954 - 962.

[104] Linde F, Nørgaard P, Hvid I, Odgaard A, Søballe K. Mechanical properties of trabecular bone. Dependency on strain rate. Journal of Biomechanics 1991;24: 803-9.

[105] Lewis G. Properties of acrylic bone cement: state of the art review. J Biomed Mater Res 1997;38: 155-82.

[106] MacNeil JA, Boyd SK. Accuracy of high-resolution peripheral quantitative computed tomography for measurement of bone quality. Med Eng Phys 2007;29: 1096-105.

[107] Kopperdahl DL, Morgan EF, Keaveny TM. Quantitative computed tomography estimates of the mechanical properties of human vertebral trabecular bone. J Orthop Res 2002;20: 801-805.

[108] Cann CE, Genant HK, Kolb FO, Ettinger B. Quantitative computed tomography for prediction of vertebral fracture risk. Bone 1985;6: 1-7.

[109] Crawford RP, Keaveny TM. Relationship between axial and bending behaviors of the human thoracolumbar vertebra. Spine 2004;29: 2248-55.

[110] Roschger P, Gupta HS, Berzlanovich A, Ittner G, Dempster DW, Fratzl P, Cosman F, Parisien M, Lindsay R, Nieves JW, Klaushofer K. Constant mineralization density distribution in cancellous human bone. Bone 2003;32: 316-23.

[111] Eckstein F, Matsuura M, Kuhn V, Priemel M, Muller R, Link TM, Lochmuller EM. Sex differences of human trabecular bone microstructure in aging are site-dependent. J Bone Miner Res 2007;22: 817-24.

[112] Lochmuller EM, Poschl K, Wurstlin L, Matsuura M, Muller R, Link TM, Eckstein F. Does thoracic or lumbar spine bone architecture predict vertebral failure strength more accurately than density? Osteoporos Int 2007;19: 537-45.

[113] Yoganandan N, Myklebust JB, Cusick JF, Wilson CR, Sances A. Functional biomechanics of the thoracolumbar vertebral cortex. Clin Biomech 1988;3: 11-18.

[114] Liu XS, Bevill G, Keaveny TM, Sajda P, Guo XE. Micromechanical analyses of vertebral trabecular bone based on individual trabeculae segmentation of plates and rods. J Biomech 2008.

[115] Mosekilde L, Viidik A, Mosekilde L. Correlation between the compressive strength of iliac and vertebral trabecular bone in normal individuals. Bone 1985;6: 291-295.

[116] Mosekilde L, Ebbesen EN, Tornvig L, Thomsen JS. Trabecular bone structure and strength - remodelling and repair. J Musculoskelet Neuronal Interact 2000;1: 25-30.

[117] Thomsen JS, Ebbesen EN, Mosekilde L. Age-related differences between thinning of horizontal and vertical trabeculae in human lumbar bone as assessed by a new computerized method. Bone 2002;31: 136-142.

[118] Liu XS, Sajda P, Saha PK, Wehrli FW, Bevill G, Keaveny TM, Guo XE. Complete volumetric decomposition of individual trabecular plates and rods and its morphological correlations with anisotropic elastic moduli in human trabecular bone. J Bone Miner Res 2008;23: 223-35.

[119] Liu XS, Bevill G, Keaveny TM, Sajda P, Guo XE. Micromechanical analyses of vertebral trabecular bone based on individual trabeculae segmentation of plates and rods. J Biomech 2009;42: 249-56.

[120] Eswaran SK, Fields AJ, Nagarathnam P, Keaveny TM. Multi-scale modeling of the human vertebral body: comparison of micro-CT based high-resolution and continuum-level models. Pac Symp Biocomput 2009: 293-303.

[121] Roux J, Wegrzyn J, Arlot M, Guyen O, Delmas P, Chapurlat R, Bouxsein M. Contribution of trabecular and cortical components to biomechanical behavior of human vertebrae: an ex-vivo study. J Bone Miner Res 2009.

[122] Stauber M, Rapillard L, van Lenthe GH, Zysset P, Müller R. Importance of individual rods and plates in the assessment of bone quality and their contribution to bone stiffness. J Bone Miner Res 2006;21: 586-95.

[123] Liu XS, Sekhon KK, Zhang XH, Bilezikian JP, Guo XE. Individual trabeculae segmentation based morphological analyses of registered HR-pQCT and μCT images of human tibial bone. In: Trans Orthop Res Soc; 2009. p. 2142.

[124] Link TM, Bauer J, Kollstedt A, Stumpf I, Hudelmaier M, Settles M, Majumdar S, Lochmuller EM, Eckstein F. Trabecular bone structure of the distal radius, the calcaneus, and the spine: which site predicts fracture status of the spine best? Invest Radiol 2004;39: 487-97.

[125] Ladinsky GA, Vasilic B, Popescu AM, Wald M, Zemel BS, Snyder PJ, Loh L, Song HK, Saha PK, Wright AC, Wehrli FW. Trabecular structure quantified with the MRI-based virtual bone biopsy in postmenopausal women contributes to vertebral deformity burden independent of areal vertebral BMD. J Bone Miner Res 2008;23: 64-74.

[126] Patel PV, Prevrhal S, Bauer JS, Phan C, Eckstein F, Lochmuller EM, Majumdar S, Link TM. Trabecular bone structure obtained from multislice spiral computed tomography of the calcaneus predicts osteoporotic vertebral deformities. J Comput Assist Tomogr 2005;29: 246-53.

[127] Kothari M, Keaveny TM, Lin JC, Newitt DC, Majumdar S. Measurement of intraspecimen variations in vertebral cancellous bone architecture. Bone 1999;25: 245-50.

[128] Wegrzyn J, Roux JP, Arlot ME, Boutroy S, Vilayphiou N, Guyen O, Delmas PD, Chapurlat R, Bouxsein ML. Role of trabecular microarchitecture and its heterogeneity parameters in the mechanical behavior of ex-vivo human L3 vertebrae. J Bone Miner Res 2010.

[129] Yeh OC, Keaveny TM. Biomechanical effects of intraspecimen variations in trabecular architecture: A three-dimensional finite element study. Bone 1999;25: 223-228.

[130] Adams MA, Dolan P. Spine biomechanics. J Biomech 2005;38: 1972-83.

[131] Adams MA, Pollintine P, Tobias JH, Wakley GK, Dolan P. Intervertebral disc degeneration can predispose to anterior vertebral fractures in the thoracolumbar spine. J Bone Miner Res 2006;21: 1409-16.

[132] Pollintine P, Dolan P, Tobias JH, Adams MA. Intervertebral disc degeneration can lead to "stress-shielding" of the anterior vertebral body: a cause of osteoporotic vertebral fracture? Spine 2004;29: 774-82.

[133] Buckley JM, Kuo CC, Cheng LC, Loo K, Motherway J, Slyfield C, Deviren V, Ames C. Relative strength of thoracic vertebrae in axial compression versus flexion. Spine J 2009;9: 478-85.

[134] Mc Donnell P, Harrison N, Liebschner MA, Mc Hugh PE. Simulation of vertebral trabecular bone loss using voxel finite element analysis. J Biomech 2009;42: 2789-96.

[135] Johnell O, Kanis JA. An estimate of the worldwide prevalence and disability associated with osteoporotic fractures. Osteoporos Int 2006;17: 1726-33.

[136] Gibson LJ. The mechanical behavior of cancellous bone. J Biomech 1985;18: 317-328.

[137] Papadopoulos P, Lu J. A general framework for the numerical solution of problems in finite elasto-plasticity. Comput Methods Appl Mech Eng 1998;159: 1-18.

[138] Papadopoulos P, Lu J. On the formulation and numerical solution of problems in anisotropic finite plasticity. Comput Methods Appl Mech Eng 2001;190: 4889-4910.

[139] Fields AJ, Lee GL, Liu XS, Jekir MG, Guo XE, Keaveny TM. Vertebral compressive strength is explained by the apparent density of the trabeculae that are vertically oriented. In: Trans Orthop Res Soc; 2010. p. 331.

[140] Fyhrie DP, Vashishth D. Bone stiffness predicts strength similarly for human vertebral cancellous bone in compression and for cortical bone in tension. Bone 2000;26: 169-73.

[141] Niebur GL, Yuen JC, Hsia AC, Keaveny TM. Convergence behavior of high-resolution finite element models of trabecular bone. J Biomech Eng 1999;121: 629-635.

[142] Guldberg RE, Hollister SJ, Charras GT. The accuracy of digital image-based finite element models. J Biomech Eng 1998;120: 289-295.

[143] Bevill G, Keaveny TM. Trabecular bone strength predictions using finite element analysis of micro-scale images at limited spatial resolution. Bone 2009;44: 579-84.

[144] Yeni YN, Christopherson GT, Dong XN, Kim DG, Fyhrie DP. Effect of microcomputed tomography voxel size on the finite element model accuracy for human cancellous bone. J Biomech Eng 2005;127: 1-8.

[145] Jaasma MJ, Bayraktar HH, Niebur GL, Keaveny TM. The effects of intraspecimen variations in tissue modulus on the apparent mechanical properties of trabecular bone. In: Trans. Orthop. Res. Soc. San Francisco; 2001. p. 513.

[146] van der Linden JC, Birkenhager-Frenkel DH, Verhaar JA, Weinans H. Trabecular bone's mechanical properties are affected by its non-uniform mineral distribution. J Biomech 2001;34: 1573-80.

[147] Verhulp E, Van Rietbergen B, Müller R, Huiskes R. Micro-finite element simulation of trabecular-bone post-yield behaviour--effects of material model, element size and type. Comput Methods Biomech Biomed Engin 2008;11: 389-95.

[148] Fyhrie DP, Schaffler MB. Failure mechanisms in human vertebral cancellous bone. Bone 1994;15: 105-9.

[149] Wachtel EF, Keaveny TM. Dependence of trabecular damage on mechanical strain. J Orthop Res 1997;15: 781-787.

[150] Magerl F, Aebi M, Gertzbein SD, Harms J, Nazarian S. A comprehensive classification of thoracic and lumbar injuries. Eur Spine J 1994;3: 184-201.

[151] Perey O. Fracture of the vertebral end-plate in the lumbar spine. Acta Orthop Scand 1957;Supplement 25: 1-101.

[152] O'Connell GD, Johannessen W, Vresilovic EJ, Elliott DM. Human internal disc strains in axial compression measured noninvasively using magnetic resonance imaging. Spine 2007;32: 2860-8.

[153] Frei H, Oxland TR, Rathonyi GC, Nolte LP. The effect of nucleotomy on lumbar spine mechanics in compression and shear loading. Spine 2001;26: 2080-9.

[154] Reilly DT, Burstein AH. The elastic and ultimate properties of compact bone tissue. J Biomech 1975;8: 393-405.

[155] Duncan NA, Lotz JC. Experimental validation of a porohyperelastic finite element model of the annulus fibrosus. In: Computer Methods in Biomechanics and Biomedical Engineering: Gordon and Breach; 1998, p. 527.

[156] Fagan MJ, Julian S, Siddall DJ, Mohsen AM. Patient-specific spine models. Part 1: Finite element analysis of the lumbar intervertebral disc--a material sensitivity study. Proc Inst Mech Eng [H] 2002;216: 299-314.

[157] Liu YK, Ray G, Hirsch C. The resistance of the lumbar spine to direct shear. Orthop Clin North Am 1975;6: 33-49.

[158] Muller R, Gerber SC, Hayes WC. Micro-compression: a novel technique for the nondestructive assessment of local bone failure. Technol Health Care 1998;6: 433-44.

[159] Fields AJ, Eswaran SK, Keaveny TM. Dependence of tissue failure in the human vertebra on volume fraction and architecture. In: Trans Orthop Res Soc. Las Vegas, NV; 2009.

[160] Pollintine P, van Tunen MS, Luo J, Brown MD, Dolan P, Adams MA. Time-dependent compressive deformation of the ageing spine: relevance to spinal stenosis. Spine 2010;35: 386-94.

[161] Wagner DR, Lotz JC. Theoretical model and experimental results for the nonlinear elastic behavior of human annulus fibrosus. J Orthop Res 2004;22: 901-9.

[162] Iatridis JC, Weidenbaum M, Setton LA, Mow VC. Is the nucleus pulposus a solid or a fluid? Mechanical behaviors of the nucleus pulposus of the human intervertebral disc. Spine 1996;21: 1174-84.

[163] Natarajan RN, Williams JR, Andersson GB. Recent advances in analytical modeling of lumbar disc degeneration. Spine 2004;29: 2733-41.

[164] Horst M, Brinckmann P. Measurement of the distribution of axial stress on the end-plate of the vertebral body. Spine 1981;6: 217-232.

[165] Grant JP, Oxland TR, Dvorak MF. Mapping the structural properties of the lumbosacral vertebral endplates. Spine 2001;26: 889-96.